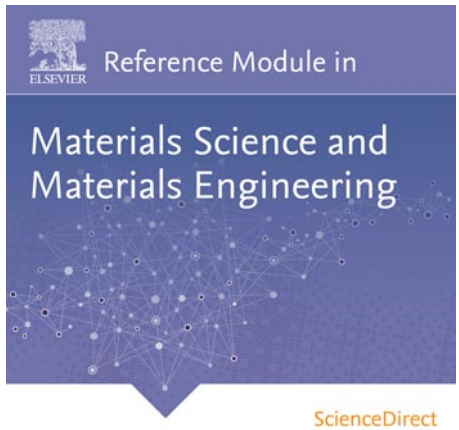

Hihara L.H., and Bakkar A., Corrosion of Metal Matrix Composites. In: Saleem Hashmi (editor-in-chief), Reference Module in Materials Science and Materials Engineering. Oxford: Elsevier; 2016. pp. 1-28.

ISBN: 978-0-12-803581-8

Corrosion of Metal Matrix Composites ☆

LH Hihara, University of Hawaii at Manoa, Honolulu, HI, USA
A Bakkar, Suez University, Suez, Egypt, and Umm Al-Qura University, Al-Lith, Saudi Arabia

☆*Change History*: October 2015. A. Bakkar changed Figures 1 and 2, new micrographs were added; Section 3 'Fabrication of MMCs' was newly added; Section 5.5 'Measuring Corrosion of MMCs,' apart from subsection 5.5.2, was newly added; Figures 24–26 was newly added. Section 5.6 was updated; New 27 references were added and 13 references were updated.

Abbreviations

B MF Boron monofilament
B_{MF}^{E} B_{MF} electrode with MF ends exposed
B_{MF}^{S} B_{MF} electrode with MF circumferential surface exposed
CD Current density
HP Hot-pressed
MMC Metal–matrix composite
SC Semiconductor
SiC MF Silicon carbide monofilament
SiC_{MF}^{E} SiC_{MF} electrode with MF ends exposed
SiC_{MF}^{S} SiC_{MF} electrode with MF circumferential surface exposed

Symbols

E Electrode with fiber or MF ends exposed (e.g., SiC_{MF}^{E})
$E_{APPLIED}$ Applied potential
E_{pit} Pitting potential
E_{GALV} Galvanic couple potential
g Gaseous state
Gr Graphite
Gr^{E} Gr electrode with fiber ends exposed
i Current density
i_a Anodic current density
i_c Cathodic current density
i_{CORR} Corrosion current density
i_{GALV} Galvanic current density
l Liquid state
s Solid state
S Electrode with fiber or MF circumferential surface exposed (e.g., SiC_{MF}^{S})
t Thickness
V_{SCE} Volts versus a calomel electrode
x_C **or** X_C Cathodic area fraction
ρ resistivity

1 Introduction

Metal–matrix composites (MMCs) are metals that are reinforced with either continuous or discontinuous constituents usually in the form of fibers (F), monofilaments (MF), particles (P), whiskers (W), or short fibers (SF). The reinforcements can be metals (e.g., tungsten, stainless steel), nonmetals (e.g., carbon, silicon), or ceramics (e.g., silicon carbide, boron carbide, or alumina). The selection of the matrix metal and reinforcement constituent is usually based on how well the combination interacts to achieve the desired properties. MMCs are usually stiff, strong, and lightweight, but they are also engineered for other properties. Reinforcements have been used in MMCs to increase stiffness,[1] strength,[1] thermal conductivity,[2] neutron shielding, and vibration damping capacity; and to reduce weight,[1] thermal expansion,[3] friction,[4] and wear.[5] Some, but not all, MMC properties are governed by the rule of mixtures.[6] Although MMCs have properties more useful than those of their individual constituents, resistance to corrosion is usually sacrificed. The corrosion behavior of MMCs is often significantly different from that of their monolithic matrix alloys because of the presence of the reinforcements that alter the microstructure, electrochemical properties, and corrosion morphology.

The different types, typical applications, corrosion characteristics, and corrosion protection of MMCs will be summarized below.

2 Types of MMCs

A variety of MMCs have been developed with matrices such as aluminum, magnesium, lead, depleted uranium, stainless steel, titanium, copper, and zinc. Only MMCs with aluminum matrices, however, are extensively available.[3] Reinforcement constituents for MMCs include boron (B), graphite (Gr), silicon (Si), silicon carbide (SiC), boron carbide (B_4C), titanium carbide (TiC), titanium diboride (TiB_2), tungsten carbide (WC), alumina (Al_2O_3), mica, quartz, tungsten, yttria, and zircon. The reinforcement constituents usually range from 10 to 60 vol%.

In this article, the MMC types will be denoted as reinforcement composition $_{\text{reinforcement type}}$ (vol%)/matrix metal or alloy. Hence, $Al_2O_{3\ P}$ (50%)/aluminum denotes an aluminum matrix MMC reinforced with 50 vol% of Al_2O_3 particles.

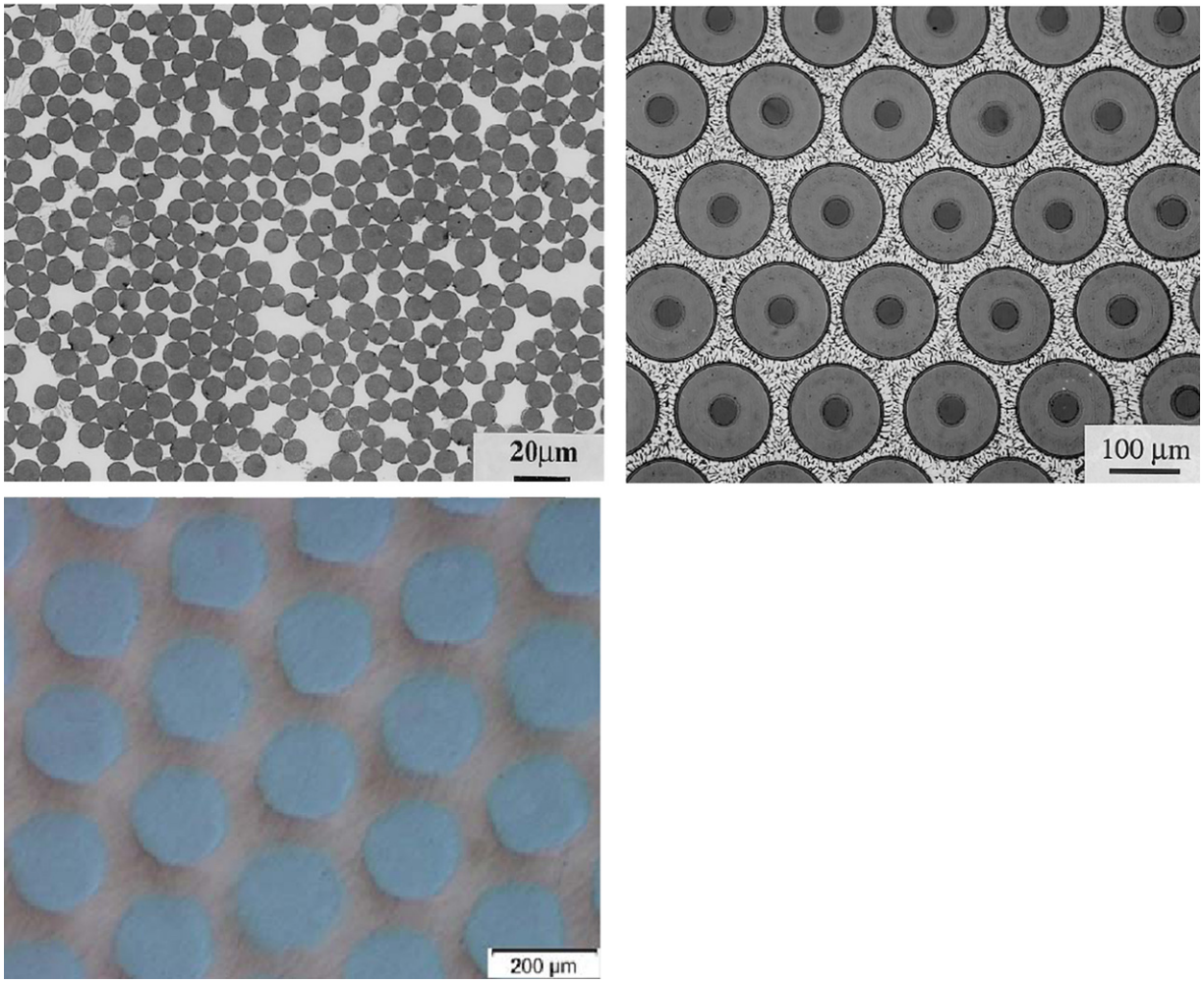

Figure 1 Micrographs of (a) C_F (55%)/Al–7Si–0.6Mg MMC,[7] (b) SiC_{MF} (67%)/Ti–6Al–2Sn–4Zr–2Mo MMC,[7] (c) stainless $steel_F$ (50%)/Cu MMC.[8]

2.1 Continuous-Reinforced MMCs

Continuous-reinforced (CR) MMCs are reinforced with continuous fibers or MF generally resulting in anisotropic properties, with substantial enhancements in the longitudinal direction of the reinforcement. The reinforcement diameter generally varies from 5 to 150 μm (**Figure 1**). Continuous reinforcements are usually much more expensive than their discontinuous counterparts. Fabrication costs of CR MMCs are also higher than that of discontinuous-reinforced (DR) MMCs.

2.2 Discontinuous-Reinforced MMCs

DR MMCs are reinforced with particles, whiskers, or short fibers (SF), and generally have isotropic properties and lower material and fabrication costs as compared to CR MMCs. Enhancements in properties of DR MMCs, however, are usually modest in comparison to CR MMCs. Reinforcement volume percents range from ~15 to 25% for structural MMCs (**Figure 2(a)**), and greater than 30% for MMCs used in electronic packaging (**Figure 2(b)**). Uniform particle and particle-size distribution are preferred in structural MMCs for optimal mechanical properties. In electronic-grade MMCs, the particle and particle-size distribution may not be uniform in order to maximize the reinforcement volume fraction. The high reinforcement loading in electronic-grade MMCs is necessary to reduce the coefficient of thermal expansion (CTE) to levels closer to that of electronic materials such as silicon and gallium arsenide. Magnesium-based MMCs, having high creep resistance, are applied in some automotive components such as gear box housing and crank cases. Hybrid Mg MMCs, based on AE42 Mg alloy reinforced by both expensive saffil-alumina (Al_2O_3) short fibers and cheap SiC particulates (**Figure 2(c)**), are developed for applications in engine components operating at temperatures above 200 °C.

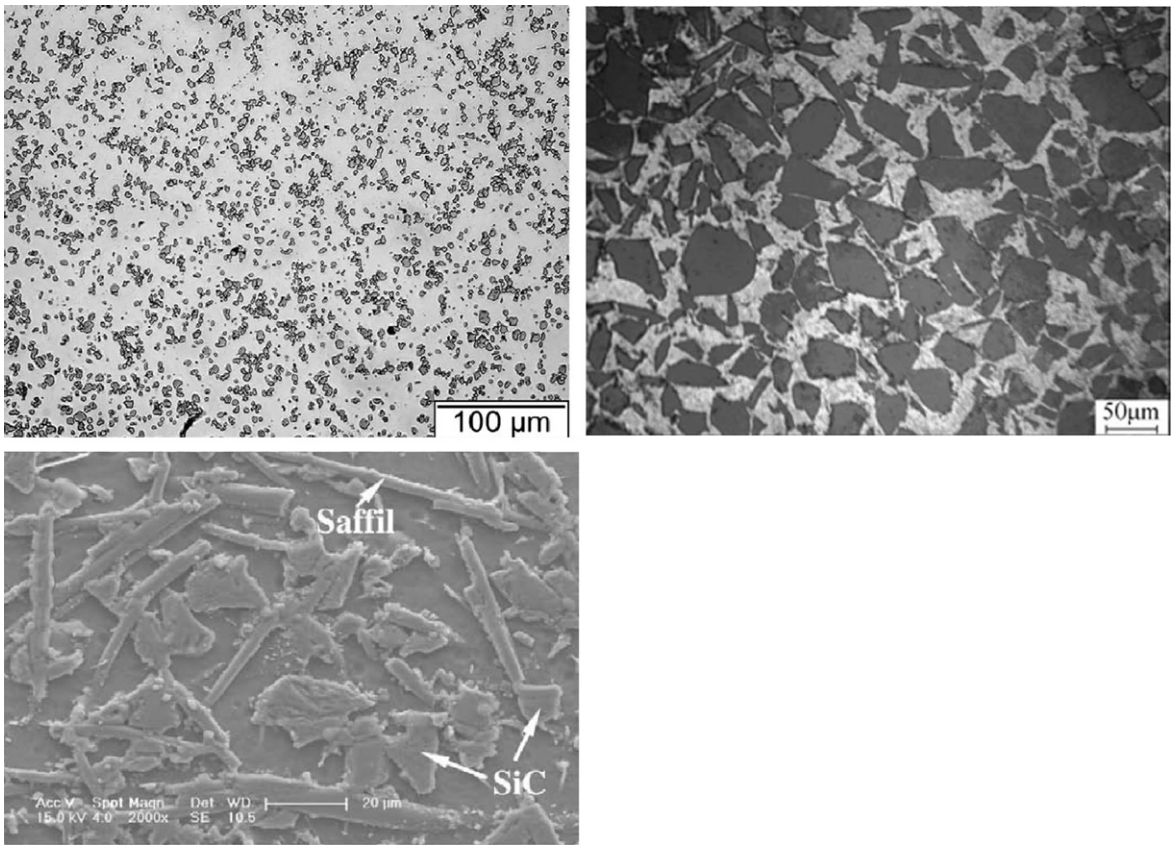

Figure 2 Micrographs of (a) $MoSi_{2\ P}$ (15%)/Al 6092 MMC,[9] (b) SiC_P (54%)/Al MMC,[10] and (c) Saffil $Al_2O_{3\ F}$(10%)/SiC_P (10%)/Mg alloy MMC.[11]

3 Fabrication of MMCs

The fabrication processing of MMC affects directly on its quality and microstructural properties and consequently on all resultant properties, comprising the corrosion behavior. Therefore, a brief description of available processing techniques for fabricating MMCs is provided below. All these processes can be generally classified into two main groups: (1) liquid phase processes, which are conducted above the melting point of the matrix, and (2) solid state processes, which operate below the melting point of the matrix. Liquid phase routes offer the advantage of firm reinforcement–matrix contact which reduces residual porosity in the final composite. Solid state processes, on the other hand, are less likely to promote the formation of adverse interfacial reaction products.

3.1 Liquid State Processes

3.1.1 Squeeze casting

Squeeze casting technique involves forcing the liquid metal into the fiber preform.[12,13] Pressure is applied by a hydraulic ram until the solidification is complete. This method is also called pressure infiltration. The advantage of applying pressure during the casting process is the elimination of gas or shrinkage porosity. Although the technique promotes good wettability of the reinforcement by the molten metal, the composites produced have minimal reaction between the reinforcement and molten metal. In addition, rapid solidification under pressure applied by the hydraulic ram, which acts also as a heat sink, leads to formation of fine equiaxed grain structure in the metal matrix. From corrosion point of view, the effect of microstructure is evident. The higher solidification rates for squeeze casting versus gravity casting cause decreased average grain sizes and decreased corrosion rates. The smaller grain size and the finer distribution of the cathodic phases, as well as the absence of porosity and interfacial phases, minimize the localized corrosion.

3.1.2 Liquid metal infiltration

Liquid metal infiltration (LMI) process[12,13] can be considered as another variant of squeeze casting. The difference is that the infiltration of preform of fibers or particles by liquid metal is provided by means of a pressurized inert gas and the process is

operated under vacuum. A preheated preform is placed into a split metal die in the shape of the component. This die is then closed, but is maintained open to a reservoir chamber of molten metal. Both the die and the metal chamber are evacuated and subsequently the melt chamber is pressurized by an inert gas, for example, argon, which forces the molten metal into the die to infiltrate the fiber preform. The pressure is kept applied until solidification occurs.

The process has the advantage of producing complex shaped components with the possibility of rather high fiber volume fractions. Another advantage over squeeze casting is that the pressures applied are greatly lower. However, a strong dependence on fiber temperature of infiltration necessitates control of the operating temperature. If the fiber temperature is too low, the solidification may occur prior to complete infiltration, thereby resulting in porosity in the composite cast. On the other hand, too high a fiber temperature results in long solidification time, and hence undesirable reactions occurring at the fiber/matrix interface are highly possible.

3.1.3 Compocasting (rheocasting)

Compocasting[12,14] is an appropriate technique for the fabrication of composites containing discontinuous reinforcement. The method involves the addition of reinforcement particles or fibers to a semi-solid matrix alloy which is undergoing vigorous stirring at a temperature between solidus and liquidus. The reinforcement is entrapped by the solid in the semi-solid slurry and it is prevented from agglomerating, settling, or floating. Continuous stirring promotes complete contact between the metal and reinforcement that improves the wettability for the reinforcement by the metal matrix. Also, The continued agitation breaks up the solidifying dendrites into spheroidal particles and prevent the rise in viscosity. The composite slurry can be directly cast into a simple billet; this is termed rheocast composite, and the process is called rheocasting. Also, the semi-solid composite mixture can be reheated to just above liquidus, in order to reduce the viscosity, and then die-cast into net shape components; this process is termed compocasting. Alternatively, the composite mixture, after pouring into a mould, can further be undergone squeeze casting process, in order to reduce the probably associated porosity.

Compocasting is a useful technique for direct fabrication of metal matrix composites without preform preparation, and it allows uniform distribution of the reinforcement in the metal matrix. However, prolonged contact between the reinforcement and molten matrix may lead to undesirable interfacial reactions which limit the process to certain reinforcement–matrix combinations.

3.1.4 Melt stirring

Melt stirring[14] is conventionally the simplest and cheapest production route for MMCs. The aimed amount of particulate reinforcement is added into a liquid metal melt and stirred until a uniform distribution of reinforcement is obtained, then the melt is cast. However, the process has some complications, such as the difficulty to wet the reinforcement and to distribute it homogeneously in the melt. Moreover, any undesirable reaction between the reinforcement and the melt is difficult to be controlled.

3.1.5 Spray co-deposition

The principle of the spray co-deposition method[14,15] depends on production of atomized stream of matrix metal, into which the reinforcement is introduced in the form of particles, whiskers, or short fibers. The metal and reinforcement are then co-deposited onto an appropriate substrate. The method has the advantage that, the short contact times during spraying limits the formation of undesirable interfacial reaction products. However, a careful control of the atomizing and reinforcement feeding is required to ensure a uniform distribution of the second phase within the matrix.

3.2 Solid State Processes

3.2.1 Powder metallurgy

The powder metallurgy[13,16] route is commonly used to produce MMCs. The process involves blending metal or pre-alloyed powder with suitable reinforcement, followed by consolidation with applying hot pressing or hot isostatic pressing. Vacuum degassing before consolidation is mostly necessary to eliminate porosity formation. Finally, secondary processing step such as extrusion or forging may be followed to provide the desired product form.

The technique gives the possibility for producing MMCs with relatively higher volume fractions of reinforcements. In addition, lower processing temperatures minimize the reinforcement-matrix interfacial reactions. A main disadvantage is that the whole operation is inherently an expensive process.

3.2.2 Diffusion bonding

Diffusion bonding, which is a solid-state welding technique, has been successfully adapted to the fabrication of MMCs. The process involves the simultaneous application of heat and static pressure, and can be generally applied to the consolidation of lay-ups of metal foils and fiber arrays, or of preformed composite monolayers. The interdiffusion of atoms, from clean metal surfaces in contact together or to the reinforcement, is responsible for creating the joint. The relatively low temperature involved gives an advantage for this technique, but the high pressures applied are likely to lead to fiber breakage. Furthermore, the process optimization is critical to achieving the desirable properties in a composite.[13,17]

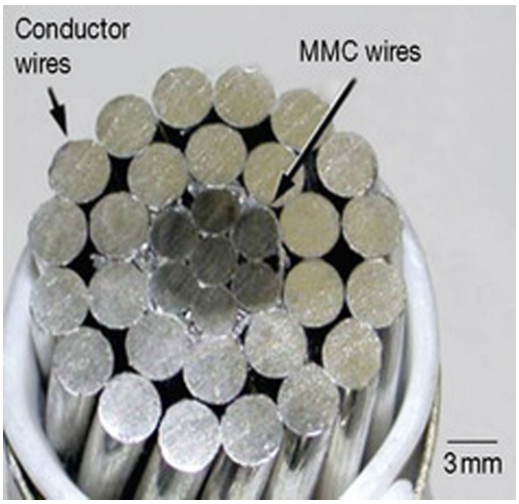

Figure 3 Aluminum conductor composite reinforced cable specimen. Notice the seven inner $Al_2O_{3\ F}$/Al MMC core wires.

4 MMC Applications

4.1 Examples of Applications for CF MMCs

B_{MF}/aluminum MMCs have been used for structural tubes in the space shuttle, resulting in 44% reduction in weight over aluminum alloys in the original design.[18] Gr_F/aluminum MMCs, which have unique properties such as negative to near-zero CTE, have been used as antenna booms in the Hubble Space Telescope.[3] In the automotive industry, $Al_2O_{3\ F}$/Al MMCs have been used to replace cast iron components. $Al_2O_{3\ F}$/Al MMCs with low weight, high temperature tensile and fatigue strengths, low thermal conductivity and expansion, and superior wear resistance are used in flywheels, engine blocks, pistons, and brake components.[19] Other types of $Al_2O_{3\ F}$/Al MMCs with low weight, high strength, and high damping capacity are used for automotive push rods, resulting in increased horsepower generation.[20] These $Al_2O_{3\ F}$/Al MMCs are also used as load-carrying core wires in high-current capacity and low-sag aluminum conductor cables (**Figure 3**). The $Al_2O_{3\ F}$/Al MMCs core wires impart desirable properties to the cable such as high strength at ambient and elevated temperatures, low CTE, and lightweight.[21] Stainless $steel_F$/copper MMCs-having a beneficial combination of high mechanical strength, high electrical conductivity and sufficient ductility at ambient and cryogenic temperatures are used as electrical conductors.[22]

4.2 Examples of Applications for DR MMCs

SiC_P (20%)/Aluminum MMCs were used to replace aluminum tubes in the catamaran 'Stars and Stripes '88,' resulting in 20 wt% savings in comparison with monolithic aluminum.[3] SiC_P (43%)/Aluminum MMCs, which are machinable, lightweight, and possess a low CTE, are used for electronic packaging (**Figure 4(a)**). For thermal management applications, copper MMCs are reinforced with milled graphite (Gr) fibers that have negative CTEs and thermal conductivities exceeding that of copper. Accordingly, the resulting Gr/Cu MMCs have lower CTEs and higher thermal conductivity than copper.[21] In the automotive sector, DR MMCs, particularly based on aluminum and magnesium matrices, are used for engine pistons, piston connection rods, rear wheel driveshafts, break calipers, cylinder liners, push rods, rocker arms, and valve guides.[23] Gr_p/Cu MMCs are developed to replace copper–lead components, to eliminate toxicity of lead and reduce weight. Gr_p/Cu MMCs have also higher wear resistance because deformation of graphite particles forms a continuous graphite film, which provide self-lubrication of the component.[23] DR MMCs are also used in the sports industry for high-performance bicycle frames and components, golf clubs, and baseball bats.[24] In the aircraft industry, examples of DR MMCs' used are fan exit guide vanes in turbine engines, ventral fins, helicopter blade sleeves (**Figure 4(b)**), and fuel access covers.[21,24] Other potential emerging applications for DR MMCs are shoes for tracked vehicles and lightweight armor. TiC_p/Ni–Cr super alloys MMCs have outstanding mechanical and physical performance even at high temperatures for refractory, abrasive, and structural applications, where upgraded resistance to wear and corrosion is aimed.[25]

5 Corrosion Characteristics

The presence of the reinforcements and the processing associated with MMC fabrication can lead to accelerated corrosion of the metal matrix. Special concerns regarding corrosion become important in MMCs as compared to the corrosion of the monolithic

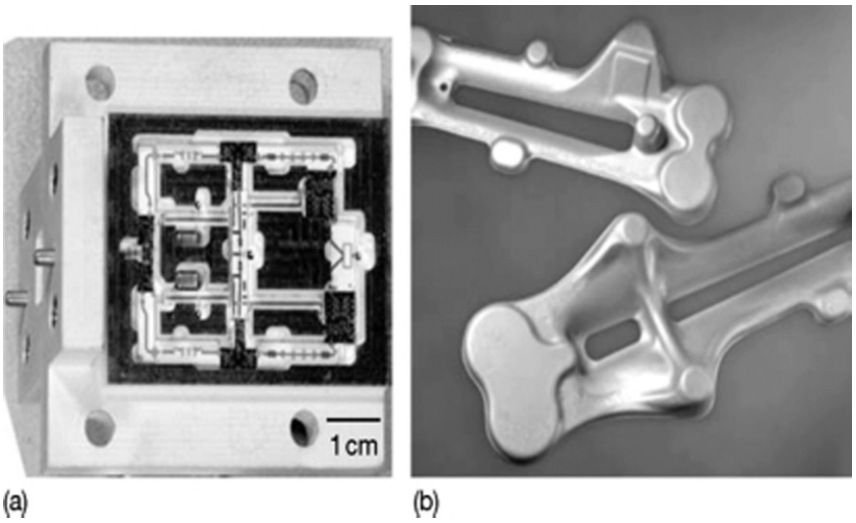

Figure 4 (a) Pure Si_P (43%)/Al MMC electronic package, and (b) 2009 SiC_P (15%)/Al–T4 MMC helicopter blade sleeves (courtesy of DWA Aluminum Composites).

matrix alloys. Accelerated corrosion in MMCs may originate from electrochemical, chemical, and physical interaction between MMC constituents because of their intrinsic properties or those induced by processing. Galvanic interaction between the reinforcement, matrix, and interphases can accelerate corrosion. Interphases and reinforcements may undergo chemical degradation, which is not electrochemical in nature. The microstructure of MMCs can influence corrosion by inducing segregation, intermetallic formation, and dislocation generation. Processing deficiencies may result in unexpected forms of corrosion.

The parameters affecting MMC corrosion that will be discussed are (1) electrochemical effects related to the primary MMC constituents; (2) electrochemical effects of the interphases; (3) chemical degradation in MMCs; and (4) secondary effects caused by the microstructure and processing. Corrosion in selected environments and corrosion protection will also be covered.

5.1 Electrochemical Effects Related to the Primary MMC Constituents

Galvanic corrosion between the matrix and reinforcements is one of the primary concerns regarding the corrosion behavior of MMCs. Depending on the electrochemical properties of the MMC constituents, the galvanic corrosion rate can be controlled by either the anodic or cathodic reaction, or by both. Anodic control prevails when the cathodic reaction is depolarized (**Figure 5(a)**); cathodic control prevails when the anodic reaction is depolarized (**Figure 5(b)**); and there is mixed control when both the anodic and cathodic reactions polarize (**Figure 5(c)**).[26] For a galvanic couple with equal matrix and reinforcement area fractions, the intersection of the anodic polarization curve of the matrix metal and the cathodic polarization curve of the reinforcement indicates the magnitude of the galvanic corrosion current density (i_{GALV}) (**Figure 6**).[27] Hence, the degree of galvanic corrosion depends on the environment, matrix alloy, reinforcement electrochemistry, resistivity, and area fraction.

5.1.1 Environment

The environment has a significant effect on galvanic corrosion rates. The two most primary factors are usually dissolved-oxygen content and electrolyte composition (e.g., presence of aggressive ions).

In deaerated environments, the governing cathodic reaction for corrosion is hydrogen evolution:

$$2H_2O + 2e^- = H_2 + 2OH^- \quad [1]$$

In aerated solutions, oxygen reduction can also operate, and generally results in higher corrosion rates:

$$O_2 + 2H_2O + 4e^- = 4OH^- \quad [2]$$

For example, if pure magnesium is coupled to an equal area of SiC_{MF} with the ends exposed (SiC_{MF}^E), the galvanic corrosion rate between Mg and SiC_{MF}^E would increase by $\sim$4 times if the solution is oxygenated (**Figure 6**). Interestingly, the normal corrosion rate of uncoupled pure magnesium does not significantly change in the presence of dissolved oxygen[27] since hydrogen evolution is the governing cathodic reaction for magnesium, as exemplified in **Figure 6**. Hence, it is important to recognize that the corrosion behavior and trends of the MMC could be significantly different than that of the monolithic matrix alloy.

The presence of aggressive ions can greatly increase the corrosion rate, especially for alloys to lose passivity. For example, the galvanic corrosion rate between a passive metal matrix and conductive reinforcements would be limited to the passive current density

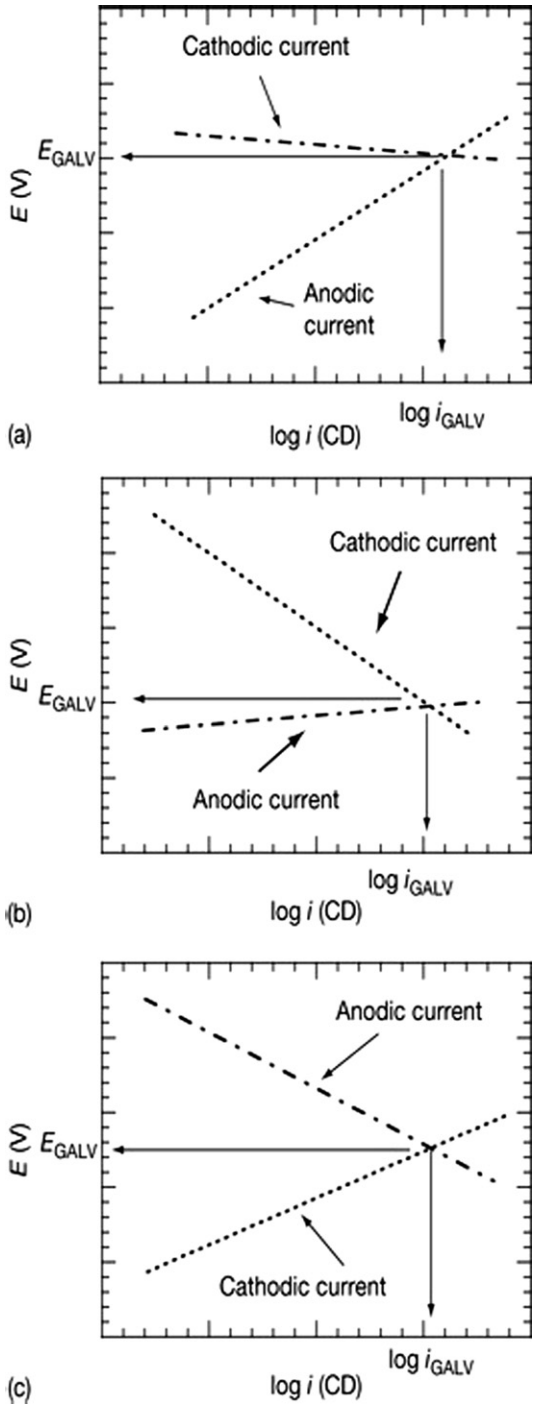

Figure 5 Polarization diagrams showing (a) anodic control, (b) cathodic control, and (c) mixed control in galvanic corrosion.

(CD), as demonstrated with the polarization diagram Al 6061-T6 plotted with those of various reinforcements in aerated chloride-free 0.5 M Na_2SO_4 (Figure 7). In the presence of aggressive ions that breakdown passivity, the galvanic corrosion rates can dramatically increase (Figure 7). Using Al 6061-T6 coupled to an equal area of P100 graphite fibers with the ends exposed (P100 Gr^E) as an example, the galvanic corrosion rate increases $\sim$300 times in aerated 3.15 wt% NaCl as compared to that in aerated 0.5 M Na_2SO_4 (Figure 7).

5.1.2 Matrix metal

Galvanic corrosion in MMCs reinforced with conductive, noble reinforcements is a concern in environments in which the matrix metal corrodes actively. For example, for MMCs reinforced with an equal area fraction of graphite fibers, i_{GALV} in aerated 3.15 wt% NaCl (Figure 8) would be only 5×10^{-7} A cm^{-2} for Ti–15 V–3Cr–3Sn–3Al (Ti-15-3), 1.5 orders of magnitude larger for pure

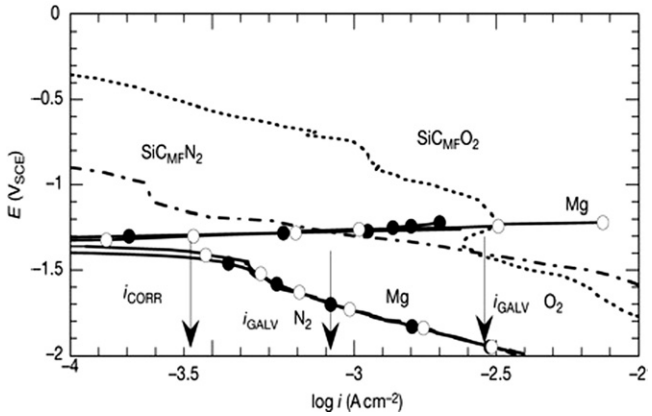

Figure 6 A collection of anodic and cathodic polarization curves of Mg (99.95%) exposed to aerated (open circles) or deaerated (solid circles) 0.5 $NaNO_3$ at 30 °C, and cathodic polarization curves of SiC_{MF}^{E} exposed to deaerated or aerated 0.5 $NaNO_3$ at 30 °C. Scan rate = 0.1 mV s^{-1}. Superscript E denotes MF ends were exposed.

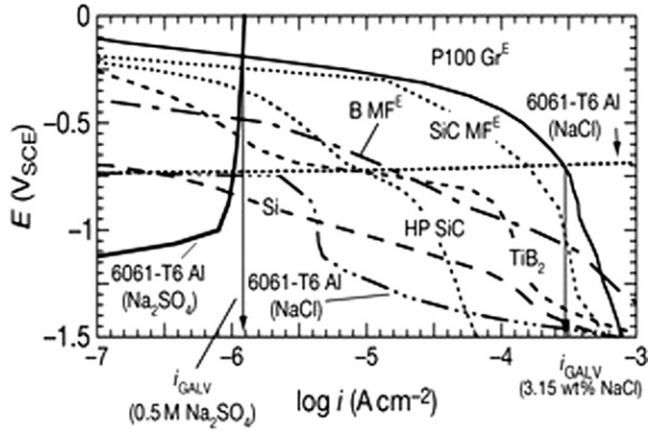

Figure 7 A collection of anodic polarization diagrams of Al 6061-T6[28] exposed to aerated 0.5 M Na_2SO_4 or 3.15 wt% NaCl at 30 °C, and cathodic polarization diagrams of P100 Gr^{E},[28] hot-pressed (HP) SiC,[28] SiC_{MF}^{E},[27] and Si,[29] TiB_2, and B_{MF}^{E} exposed to aerated 3.15 wt% NaCl at 30 °C. Scan rate = 0.1 mV s^{-1}.

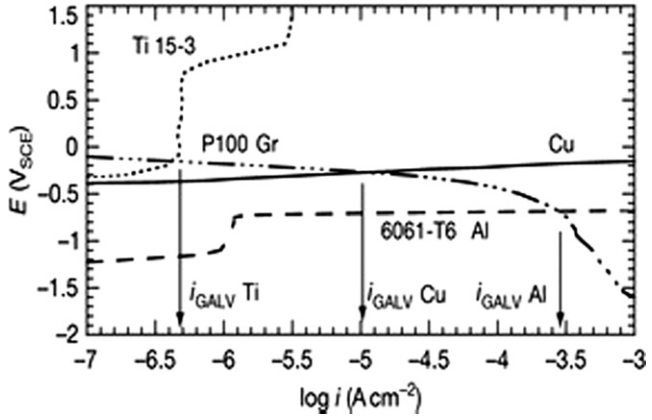

Figure 8 Anodic polarization diagrams of Ti-15-3,[30,31] pure Cu (99.999%), and Al 6061-T6[28] in deaerated 3.15 wt% NaCl at 30 °C. Cathodic polarization diagram of P100 Gr fibers[28] in aerated 3.15 wt% NaCl at 30 °C. Scan rate = 0.1 mV s^{-1}.

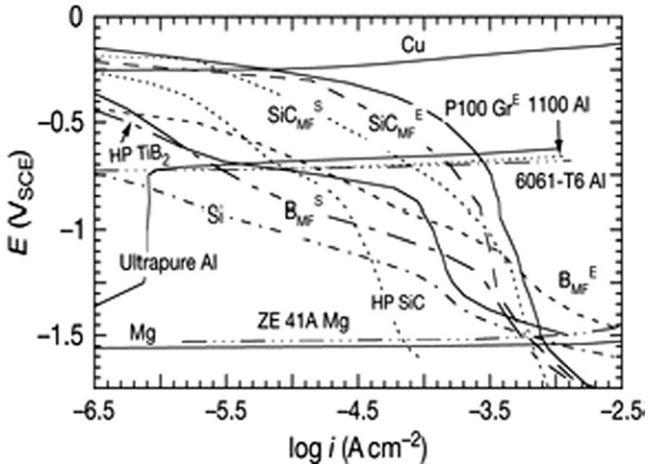

Figure 9 A collection of anodic polarization diagrams of ultrapure Al (99.999%),[28] Al 1100,[29] and Al 6061-T6,[28] and cathodic polarization diagrams of P100 Gr^{E},[28] HP SiC,[28] $SiC_{MF}{}^{E}$,[32] $SiC_{MF}{}^{S}$,[32] Si,[29] $B_{MF}{}^{E}$,[33] and $B_{MF}{}^{S}$ [33] exposed to aerated 3.15 wt% NaCl at 30 °C. Scan rate = 0.1 mV s^{-1}.

copper (10^{-5} A cm^{-2}), and 3 orders of magnitude larger for Al 6061-T6 (3×10^{-4} A cm^{-2}). The passivity of Ti-15-3 prevents i_{GALV} from exceeding the passive-CD (**Figure 8**). In the case of pure copper, i_{GALV} is about 1 order of magnitude less than the normal copper corrosion CD (10^{-4} A cm^{-2}) in the aerated 3.15 wt% NaCl; hence, galvanic action would increase corrosion of copper, but not significantly.

5.1.3 Reinforcement electrochemistry

In cases where galvanic corrosion is under cathodic control, the type of reinforcement may have a significant effect on the rate of galvanic corrosion. For example, in aluminum MMCs, the galvanic corrosion rates between Al 6061-T6 and various reinforcements ranked from the highest to lowest in aerated 3.15 wt% NaCl is as follows (**Figure 9**): P100 Gr > carbon-cored $SiC_{MF}{}^{E}$ with ends exposed > tungsten-cored $B_{MF}{}^{E}$ with ends exposed > hot-pressed (HP) SiC > Si. It should also be noted that ceramic reinforcements may vary in purity and structure, and some reinforcements are in themselves composites. This leads to interesting electrochemical behavior. For example, SiC MFs have carbon-rich outer layers and carbon cores, and their polarization diagrams have a stronger resemblance to P100 Gr^{E} than to HP SiC. The orientation of reinforcements may also affect electrochemical behavior. SiC MFs have carbon cores and B MFs have tungsten cores. The polarization behavior of the circumferential surface of the MFs are different compared with the behavior of the ends of the MFs that expose the carbon and tungsten cores (**Figure 9** compares cathodic curves for SiC MF^{S} versus SiC MF^{E}, and B MF^{S} versus B MF^{E}).

Therefore, the composition of the reinforcement is important to the extent that it affects the kinetics of hydrogen evolution and oxygen reduction. For reinforcements of very high resistivity, galvanic corrosion can also be limited by a large ohmic drop through reinforcement.

5.1.4 Reinforcement photoelectrochemistry

If the MMC reinforcements or constituents are semiconductors (SCs), galvanic currents between the matrix metal and SC could be suppressed or accelerated depending on whether the SC is n-type or p-type, respectively.[34]

5.1.4.1 n-Type SCs

An n-type semiconductor is photoanodic, and under illumination promotes photooxidation reactions. One such reaction is the oxidation of water. In the presence of moisture and illumination on MMCs that contain n-type SCs, photogenerated electrons could polarize the MMC to more negative potentials inducing cathodic protection (**Figure 10**).[34] While the MMC is under illumination, E_{corr} shifts from E_{corr} (dark) to E_{corr} (illum), and the dissolution from the matrix decreases from i_{matrix} (dark) to i_{matrix} (illum). Accordingly, during anodic polarization of $Al_2O_{3\ P}$ (20%)/Al 6092-T6 MMCs that were immersed in air-exposed 0.5 M Na_2SO_4 solutions, anodic current densities increased sharply during illumination which were attributed to photoanodic currents generated by water oxidation on TiO_2 particles that were likely introduced with the Al_2O_3 reinforcements.[35,36] The open-circuit potentials also decreased upon illumination. In these MMCs exposed to outdoors, corrosion films were also thinner on the topside of specimens exposed to sunlight as compared with the backside of the specimens not exposed to sunlight.[37] Interestingly, MMCs containing p-type SCs had thicker corrosion films on the sunlit surfaces as opposed to the shaded surfaces.[37]

5.1.4.2 p-Type SCs

A p-type SC is photocathodic and under illumination promotes photoreduction reactions. Depending on the electrolyte conditions, proton or oxygen reduction may be enhanced at the p-type semiconductor. In the presence of moisture and illumination on

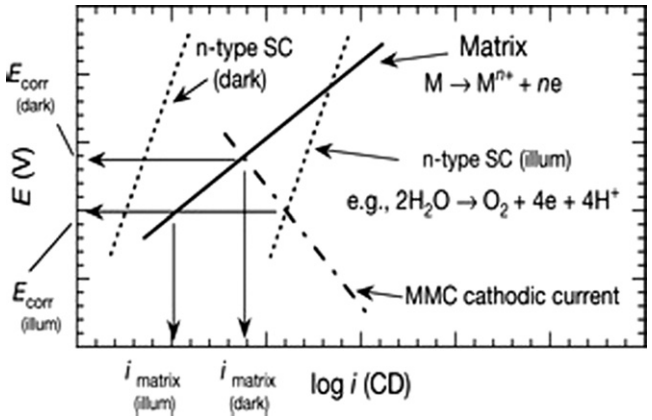

Figure 10 Polarization diagrams showing the effect of an illuminated n-type semiconductor (SC) on the corrosion current density (CD) of the MMC matrix.

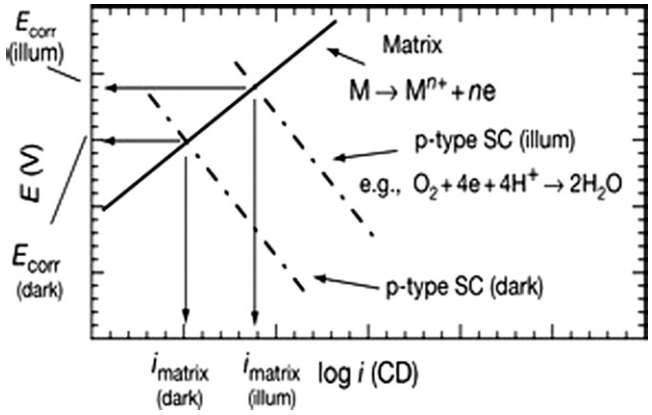

Figure 11 Polarization diagrams showing the effect of an illuminated p-type SC on the corrosion CD of the MMC matrix.

MMCs that contain p-type SCs, photoreduction causes cathodic current to increase, raising the corrosion potential and corrosion rates (Figure 11).[34] While the MMC is under illumination, E_{corr} shifts positive from E_{corr} (dark) to E_{corr} (illum), and the dissolution from the matrix increases from i_{matrix} (dark) to i_{matrix} (illum). Accordingly, during cathodic polarization of pure Si_P (43%)/Al MMCs[38] and various of SiC $_P$/Al 6092-T6 MMCs[34] that were immersed in air-exposed 0.5 M Na_2SO_4 solutions, cathodic current densities increased sharply during illumination, which were attributed to photocathodic currents on the Si or SiC particles. The open-circuit potentials also increased upon illumination.[34] In these MMCs exposed to outdoors, corrosion films were also thicker on the sunlit surfaces as opposed to the shaded surfaces.[37]

5.1.5 Reinforcement resistivity

Reinforcement materials generally fall into the categories: insulators, semiconductors (SCs), or conductors (Table 1). For reinforcements that are insulators, galvanic corrosion is not possible. For SCs, the degree of galvanic corrosion will be restricted by the magnitude of ohmic losses through the reinforcements. This is demonstrated[33] by plotting (Figure 12) the cathodic curve derived from the hydrogen evolution on P100 Gr[39] exposed to aerated 3.15 wt% NaCl at 30 °C and incorporating a term for hypothetical ohmic losses through the electrode (eqn [3]).

$$E_{APPLIED}(V_{SCE}) = -0.67 - 0.081 \times \log i + i\rho t \quad [3]$$

The ohmic loss term $i\rho t$ corresponds to a planar electrode having a thickness t and resistivity ρ, and one-dimensional current flow through the thickness. Equation [3] was plotted for various resistivity values and an electrode thickness of 5 μm with that of anodic polarization diagrams of copper, Al 6061-T6, ZE 41A Mg, and pure magnesium in 3.15 wt% NaCl. Notice the effect of ohmic losses on the cathodic polarization diagrams and decreasing galvanic current densities as the reinforcement resistivities increase (Figure 12). For example, i_{GALV} of Al 6061-T6 is $\sim 10^{-4}$ A cm^{-2} for an ohmic loss IR_1 resulting from a reinforcement resistivity of 10^7 Ω cm. The value of i_{GALV} reduces to $\sim 10^{-7}$ A cm^{-2} when the ohmic loss is increased to IR_2 by a reinforcement

Table 1 Resistivities of reinforcement materials

Material	*Resistivity (Ω cm)*	*Temperature (°C)*	*Notes*	*Reference*
Al_2O_3	$>10^{14}$	30	99.7% Al_2O_3	42
Mica	10^{13}–10^{17}	–	Muscovite $KAl_3Si_3O_{10}(OH)_2$	43
SiC	10^{-5}–10^{13}	–	Function of purity	40
B	6.7×10^5	25	Pure	44
B_4C	10^0			45
Si	10^{-2}–10^5	–	Function of purity	42
P100 Gr fiber	2.5×10^{-4}	–	Thornel	46
P55S Gr fiber	7.5×10^{-4}	–	Thornel	46
SiC_{MF}^{E}	4×10^{-2}	25	The superscript 'E' indicates that electrical contact was made with the end of the MF exposing the core; the 'S' indicates that electrical contact was made with only the MF circumferential surface (excluding the core). SiC MFs have carbon cores and B MFs have tungsten cores	33
SiC_{MF}^{S}	2×10^{-2}	25		
B_{MF}^{E}	2×10^{-1}	25		
B_{MF}^{S}	5×10^{-1}	25		

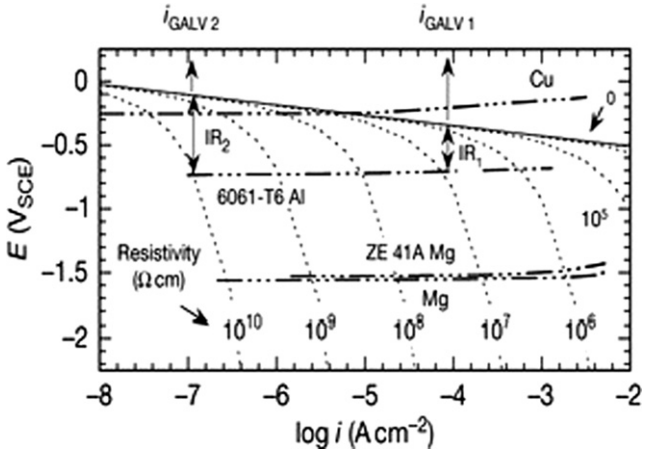

Figure 12 Plots of the Tafel equation for oxygen reduction on P100 Gr^E incorporating the effect of hypothetical ohmic losses based on various resistivities eqn [3] in aerated 3.15 wt% NaCl at 30 °C.[33] The anodic polarization diagrams of Cu, Al 6061-T6,[28] pure Mg, and ZE 41A Mg are also shown. The pure Mg and ZE41A Mg diagrams correspond to oxygenated solutions. Scan rate = 0.1 mV s^{-1}.

resistivity of 10^{10} Ω cm. The effect of reinforcement resistivity on the galvanic corrosion rate is also dependent on the type of matrix metal. The limiting effect on galvanic corrosion rates on copper only manifests at very high reinforcement resistivities (e.g., $>10^7$ Ω cm in **Figure 12**); whereas, effects are seen on Al 6061-T6, ZE 41A Mg, and magnesium at lower resistivities. Note that the i_{GALV} values correspond to galvanic couples having equal anode and cathode areas.

Figure 12 is based on a fixed electrode thickness, but note that the critical resistivity to limit the galvanic corrosion rate below a particular level is also dependent on the thickness of the reinforcement since the ohmic loss is equal to $i\rho t$. Hence, if ohmic losses are to limit galvanic corrosion, reinforcements having higher resistivity are needed as the thickness or particle size of the reinforcement decreases. For example, to maintain an ohmic drop of 0.5 V at a galvanic CD of 10^{-4} A cm^{-2}, a 50 μm particle would need a resistivity of 10^6 Ω cm; whereas, a 5 μm particle would need a resistivity of 10^7 Ω cm to achieve the same ohmic loss. If the reinforcements that are used in MMCs are not of high purity, resistivities may drop significantly allowing galvanic corrosion to ensue. For example, Al/SiC MMCs are fabricated from both high-purity green SiC and lower-purity black SiC, depending on the application. The resistivity of SiC may vary by ~18 orders of magnitude depending on its purity.[40] Boron MFs are more conductive than pure boron due to tungsten and tungsten borides in the core.[41] In fact, many reinforcement materials have resistivities that are not high enough to stifle galvanic corrosion. The resistivities of some reinforcement materials are shown in **Table 1**. The treatment above for the ohmic losses through reinforcement particles should only be considered as an approximation since one-dimensional current flow was assumed. In the actual case, the ohmic drop through the edges of the particle could be much less than through the thickness. The galvanic corrosion rate can also significantly increase as the area fraction of the reinforcements increases.

5.1.6 Reinforcement area fraction

The galvanic corrosion rate generally increases with the area fraction of the reinforcement. This is demonstrated (Figure 13) using the anodic polarization diagrams of copper, Al 1100, Al 6061-T6, pure magnesium (99.95% metallic purity), and ZE 41 A Mg, and the cathodic polarization diagram of P100 Gr.[28] The cathodic curve for P100 Gr^E shifts to higher currents as its area fraction is increased, causing the galvanic current with the various metals and alloys to increase. Since the galvanic couples are predominately under cathodic control, the catchment area principle[47] can be used to determine i_{GALV} as a function of the area fraction of the cathodic reinforcement.[28]

$$i_{GALV} = i_C(X_C/1 - X_C) \quad [4]$$

The parameter i_{GALV} is the dissolution CD of the matrix (i.e., i_{GALV}/anode area); i_C is the CD of the cathode; X_C is the area fraction of the cathode; and $(1 - X_C)$ is the area fraction of the anode. The value of i_C can be set equal to the CD of the cathodic constituents at the galvanic couple potential. For example, the galvanic couple potentials of ultrapure aluminum, Al 1100, and Al 6061-T6 couple to various reinforcements are coincident with the pitting potentials of the aluminum alloys (i.e., $\sim -0.75\ V_{SCE}$). Hence, the values of i_C for a variety of reinforcements were read at $\sim -0.75\ V_{SCE}$ from Figure 7. By plotting eqn [4] a graph (Figure 14) was generated from which i_{GALV} of ultrapure aluminum, Al 1100, or Al 6061-T6 can be obtained as a function of the area fraction of P100 Gr^E, SiC MF^E, B MF^E, HP SiC, and Si with exposure to aerated 3.15 wt% NaCl at 30 °C.[33] Figure 14 shows that to sustain a galvanic corrosion rate equal to the normal corrosion rate of Al 6061-T6, it would take less than 0.05 area fraction of P100 Gr^E or SiC MF^E, between 0.2 and 0.3 area fraction of B MF^E and HP SiC, and more than 0.9 area fraction of Si. It should be noted that for those reinforcements for which i_C was read in the diffusion-limited regime for oxygen reduction, galvanic

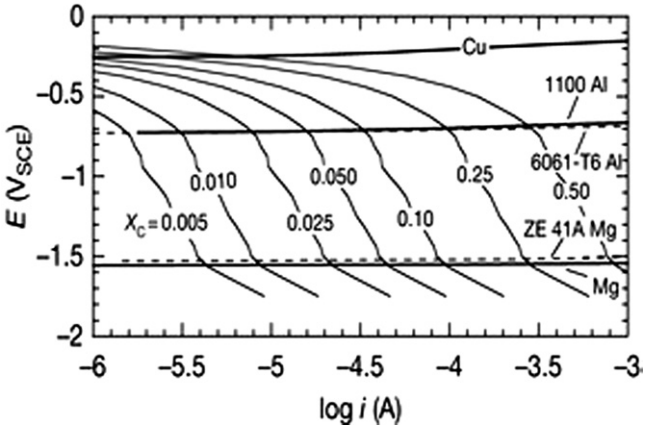

Figure 13 Anodic polarization diagrams of Cu, Al 1100, Al 6061-T6, Mg, and ZE 41A Mg, and cathodic polarization diagrams of P100 Gr^E[28] showing the effect of the P100 Gr^E area fraction X_C on the galvanic current in aerated 3.15 wt% NaCl at 30 °C. Scan rate = 0.1 mV s^{-1}.[33] The electrode area of the anodic diagrams corresponds to 1 cm^2.

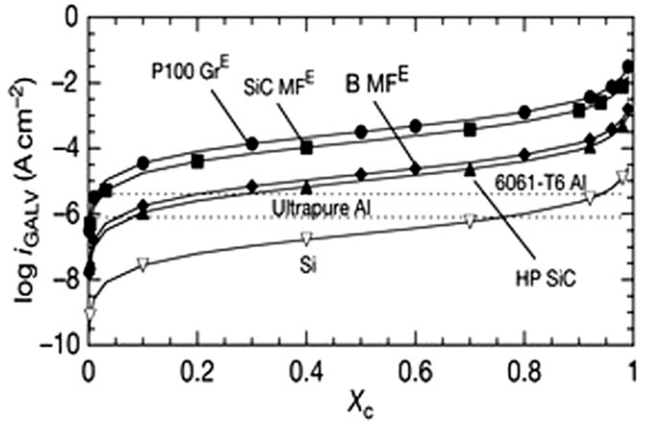

Figure 14 Graphs showing the galvanic corrosion current density i_{GALV} of ultrapure Al (99.999%), Al 1100, or Al 6061-T6 as a function of the area fraction X_C of P100 Gr^E, SiC MF^E, B MF^E, HP SiC, and Si for exposure to aerated 3.15 wt% NaCl at 30 °C. The horizontal dashed lines represent the normal corrosion rates of ultrapure Al and Al 6061-T6. Reproduced from Ref. 33.

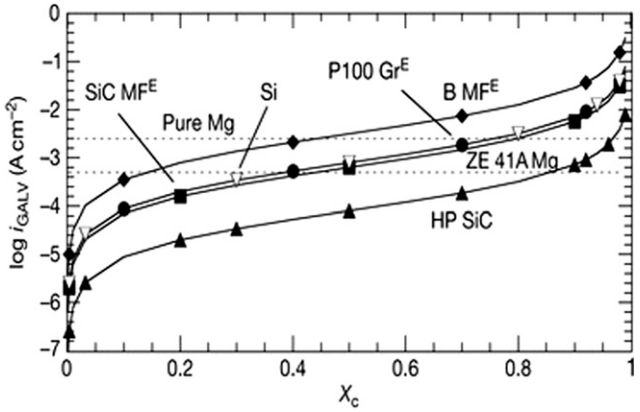

Figure 15 Graphs showing the galvanic corrosion current density i_{GALV} of pure Mg and ZE 41A Mg as a function of the area fraction X_C of P100 Gr^E, SiC MF^E, B MF^E, HP SiC, and Si for exposure to aerated 3.15 wt% NaCl at 30 °C. The horizontal dashed lines represent the normal corrosion rates of pure Mg and ZE 41A Mg.

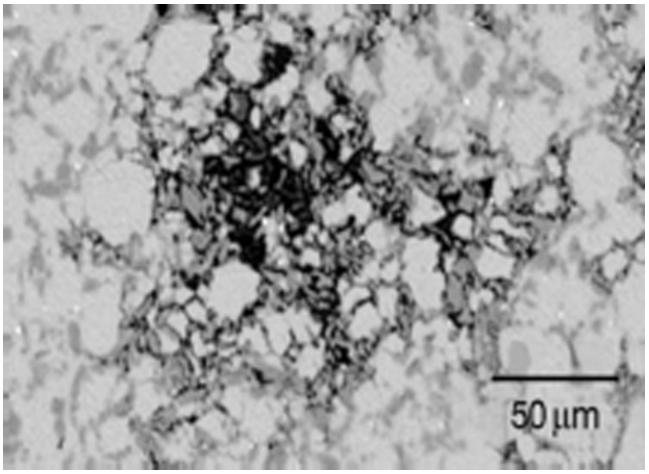

Figure 16 SEM micrograph of region of localized corrosion on SiC_P (20%)/Al 6092-T6 MMC exposed for 24 h in aerated 0.5 M Na_2SO_4 at 30 °C in the open-circuit condition. Micrograph courtesy of H. Ding.

corrosion rates could increase with additional convection. A similar figure was developed for pure magnesium and ZE 41A Mg (**Figure 15**).

The above discussion did not take into consideration the distribution of the anodic and cathodic current densities over the MMC microstructure. In some cases, for very low levels of conductive particles, localized corrosion can be induced by solution alkalinization, as will be discussed below.

5.1.7 Microstructure

The physical presence of the reinforcements also greatly affects MMC corrosion. The reinforcements, which are usually inert in comparison to the matrix, are often left in relief as the matrix corrodes leaving behind a network of fissures that trap corrosion products and exacerbate corrosion (**Figure 16**). The initiation and propagation of corrosion sites are generally influenced by the electrical resistivity and volume fraction of the MMC constituents, including the reinforcements, interphases, and intermetallics. The corrosion behavior of MMCs in the open-circuit condition can be quite different from what might be expected based on anodic polarization diagrams of the MMCs. For example, in near-neutral 0.5 M Na_2SO_4 solutions, various aluminum MMCs passivate (**Figure 17**)[48,49] during anodic polarization, but in the open-circuit condition, the same MMCs are susceptible to localized corrosion. The localized corrosion in the open-circuit condition is caused by the development of localized anodic and cathodic sites. The alkalinity in cathodic regions and acidity in anodic regions are accentuated by the formation of microcrevices in the network of reinforcement particles in relief. In the case of Al MMCs, aluminum loses its passivity in both the acidic and alkaline environments because of the amphoteric nature of aluminum oxide.

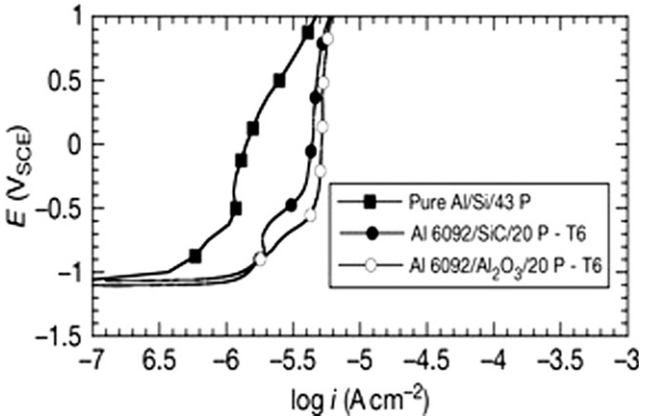

Figure 17 Anodic polarization curves of various Al MMCs exposed to 0.5 M Na_2SO_4 at 30 °C. Scan rates are 1 mV s^{-1} for Al 6092-T6 MMCs and 0.1 mV s^{-1} for Si_P (43%)/Al MMC 'pure Al/Si/43 P.'

Table 2 Values[a] of i_c as a function of x_c

i_c (A cm^{-2})	x_c
4×10^{-3}	0.001
4×10^{-4}	0.01
1×10^{-4}	0.04
4×10^{-5}	0.1
2×10^{-5}	0.2
9×10^{-6}	0.3
4×10^{-6}	0.5

[a] i_c values correspond to $i_a = 4 \times 10^{-6}$ A cm^{-2}.

When an MMC is exposed to an electrolyte in the open-circuit condition, the sum of anodic current I_a is equal to the sum of cathodic current I_c:

$$I_a = I_c \quad [5]$$

Hence, the anodic and cathodic current densities are related by eqn [6][48]

$$i_c = i_a \frac{(1 - x_c)}{x_c} \quad [6]$$

where i_c and i_a are the cathodic and anodic current densities, respectively, and x_c is the area fraction of cathodic constituents, here assumed to be conductive reinforcement, interphase, or intermetallic particles.

From eqn [6] the cathodic CD over cathodic constituents in the MMC microstructure can be approximated if the anodic CD of the matrix i_a, and the area fraction of cathodic constituents x_c are known. Experimental results on Al MMCs have indicated that the corrosion initiation sites depended on the amount of electrically conductive cathodic constituents that are present in the MMC microstructure. If the area fraction of cathodic constituents were low, corrosion initiated around the cathodic constituents because of solution alkalinization; if the area fraction of cathodic constituents were high, corrosion initiation appeared more random around the reinforcement constituents.

Equation [6] was used to calculate the cathodic CD (**Table 2**) emanating from cathodic sites based on the area fraction x_c, and the assumption that the passive CD of the aluminum matrix was $\sim 4 \times 10^{-6}$ A cm^{-2}, based on the passive CD of various Al 6092-T6 MMCs (**Figure 17**). This passive CD should also be approximately equal to the initial anodic CD i_a of the Al matrix in the MMC at the open-circuit potential, prior to the development of significant pH gradients.

5.1.7.1 Low content of cathodic constituents

When the amount of cathodic sites is relatively low, cathodic current densities become concentrated over the few cathodic sites resulting in hydroxide ion buildup. If the matrix material is not stable at high pH levels, localized corrosion can result. **Table 2** shows the values of i_c as a function of x_c, assuming a value for i_a to be equal to 4×10^{-6} A cm^{-2}, which is an estimate of the passive CD of an Al 6092-T6 matrix.

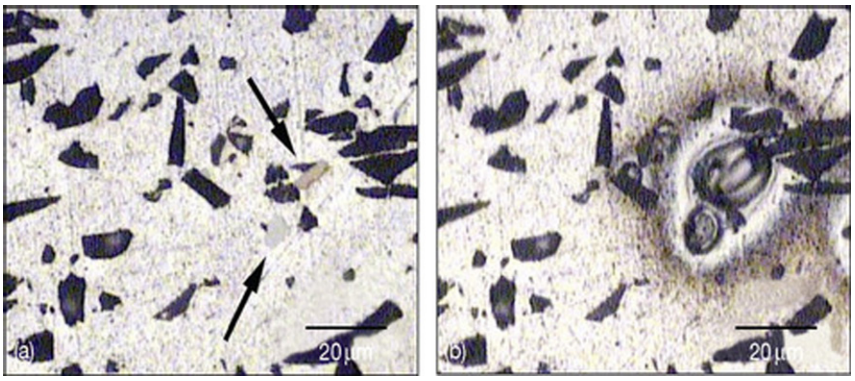

Figure 18 Virgin $Al_2O_{3\ P}$ (20%)/Al 6092-T6 MMC (a) and after 2 days of immersion (b) in air-exposed 0.5 M Na_2SO_4 at 30 °C. Intermetallic particles appear as light gray, and Al_2O_3 appears as near black.

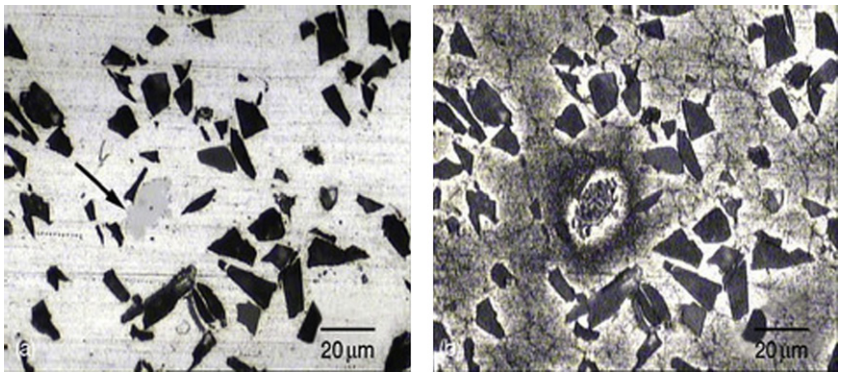

Figure 19 $Al_2O_{3\ P}$ (20%)/Al 6092-T6 MMCs in the virgin state (a) and after immersion for 17 days in air-exposed pH 7 buffered solution at 30 °C (b). Notice staining of the matrix around the intermetallic particle, but lack of localized corrosion.

When values of x_c become less than ~0.04 (**Table 2**), the cathodic current densities begin to exceed 10^{-4} A cm^{-2}, which can lead to solution alkalinization by oxygen reduction and hydrogen evolution. Cathodic current densities of the order of 10^{-4} A cm^{-2} causes phenolphthalein dye in 0.5 M Na_2SO_4 solutions to transform from clear to red for electrodes in quiescent solutions. The color change of phenolphthalein occurs in a pH range from 8.3 to 9.8. Aluminum corrosion rates increase exponentially when the pH exceeds ~8.[50] Hence, corrosion can be expected around cathodic constituents if their area fractions are low.

Accordingly, corrosion was observed on an $Al_2O_{3\ P}$ (20%)/Al 6092-T6 MMCs around intermetallic particles (**Figure 18**) in 0.5 M Na_2SO_4, in which Al passivates during anodic polarization.

In these MMCs, the Al_2O_3 particles are insulators and cannot serve as cathodes. However, several types of particles including titanium oxides and titanium suboxides, Ti–Zr–Al containing oxides, and Fe–Si–Al intermetallics- were found.[36] Of these particles, the titanium suboxides, TiO_2, and the Fe–Si–Al intermetallics supported significant cathodic activity.[36] The area fraction of the non-Al_2O_3 particles in the MMCs was estimated to be of the order of 0.01 using image analysis.[48] Hence, if the area fraction of the cathodic constituents was less than 0.01, cathodic current densities in excess of 10^{-4} A cm^{-2} could result in significant solution alkalinization and corrosion.

The scanning vibrating electrode technique (SVET) and scanning ion-selective electrode technique (SIET) revealed that localized corrosion over $Al_2O_{3\ P}$ (20%)/Al 6092-T6 MMCs immersed in 0.5 M Na_2SO_4 was coinciding with that in alkaline, cathodic regions.[51]

The type of corrosion discussed above was suppressed in pH 7 buffered solutions. Only staining was observed around the intermetallics (**Figure 19**).

5.1.7.2 High content of cathodic constituents

MMCs that contain relatively high levels of cathodic sites should generally be more immune to corrosion initiation caused by extensive hydroxide ion buildup around the cathodic constituents, since the cathodic current is dispersed over more sites.

For example, in Al MMCs that are exposed to Na_2SO_4 solutions in which the Al matrix passivates, the cathodic current densities are estimated to be relatively low (i.e., $\leq 4 \times 10^{-5}$ A cm^{-2}) (**Table 2**) for x_c greater than ~0.1. Accordingly, corrosion initiation

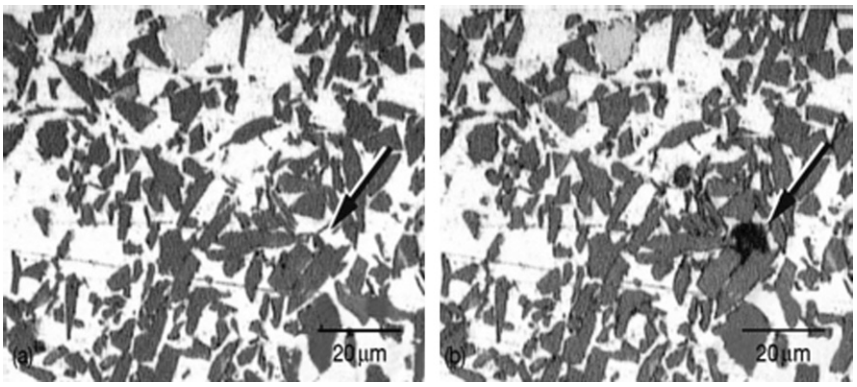

Figure 20 SiC_P (40%)/Al 6092-T6 MMC in the virgin state (a) and after immersion for 2 days (b) in air-exposed 0.5 M Na_2SO_4 at 30 °C.

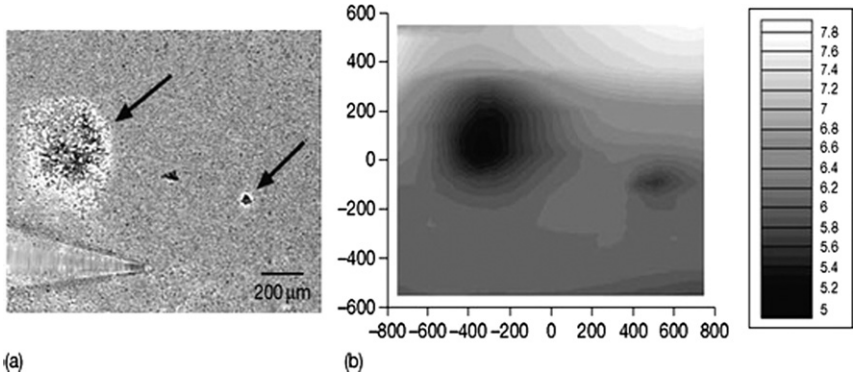

Figure 21 SiC_P (20%)/Al 6092-T6 MMC in air-exposed 0.5 M Na_2SO_4 (a), and pH profile over the specimen (b). Notice acidification of localized corrosion sites, and the alkalinization of surrounding cathodic sites.

sites on Al 6092-T6 MMCs reinforced with semiconductive SiC (Figure 20) and B_4C (greater than 10 vol%) were different in appearance from the alkali-induced corrosion around intermetallics (Figure 18) in the $Al_2O_{3\ P}$ (20%)/Al 6092-T6 MMC.[48]

One possible source of the corrosion initiation sites on the Al 6092-T6 MMCs reinforced with SiC or B_4C could be the formation of crevices at SiC–Al or B_4C–Al interfaces by the hydrolysis of Al_4C_3, which is a reaction product of SiC and Al,[52] and B_4C and Al.[53] Al_4C_3 readily hydrolyzes upon contact with moisture and could leave fissures in the SiC–aluminum and B_4C–aluminum interface (see Section 5.4.3).

Once a crevice is formed at the particle–matrix interface, crevice corrosion can ensue. If the reinforcement particles are electrically conductive, they can serve as cathodic sites for hydrogen and/or oxygen reduction. As a result, for Al MMCs, the environment in the crevice will become acidic:

$$Al \rightarrow Al^{3+} + 3e^- \quad [7]$$

$$Al^{3+} + \frac{3}{2}H_2O \rightarrow \frac{1}{2}Al_2O_3 + 3H^+ \quad [8]$$

The acidified solution in the crevice can breakdown passivity because of the amphoteric nature of Al_2O_3 and exacerbate corrosion. Eventually, corrosion spreads and encompasses adjacent particles forming a network of microcrevices caused by reinforcement particles in relief (Figure 21). The solution above the network of microcrevices has been measured to be acidic in the initial stages of growth.[51] The region around the centralized anodic region becomes alkaline because of the reduction of oxygen in surrounding regions.[51]

5.2 Electrochemical Effects of the Interphases

During the fabrication processing of MMCs, reactions between the reinforcement and matrix may lead to the formation of an interphase at the reinforcement–matrix interface. The presence of the interphase may lead to corrosion behavior different from

what might be expected based on virgin MMC constituents. For example, Pohlman[54] could not measure galvanic currents between virgin B MFs and Al 2024 or Al 6061 in 3.5% NaCl solutions, indicating that galvanic corrosion between aluminum matrices and B MFs should be negligible. In actual B_{MF}/Al MMCs, however, galvanic corrosion takes place between the aluminum matrix and the aluminum boride interphase on the surface layers of the B MFs.[54] Pohlman measured galvanic currents between the aluminum alloys and B MFs that were extracted from the matrix. A 4 μm-thick layer of aluminum boride enveloped the extracted B MFs. Galvanic currents measured between the aluminum alloys and aluminum boride were similar to those between the alloys and the extracted B MFs. When the layer of aluminum boride was removed from the extracted B MFs, the galvanic current ceased, which indicated that the aluminum boride interphase was necessary for galvanic corrosion.

5.3 Chemical Degradation in MMCs

MMCs may also degrade by chemical reactions that cannot be directly assessed by electrochemical measurements. Interphases and reinforcement phases may undergo chemical degradation which cannot be detected, for example, with the aid of anodic polarization. In aluminum MMCs, the hydrolysis of the Al_4C_3 interphase is one such example. Aluminum carbide degradation can affect Gr/Al, SiC/Al, and B_4C/Al MMCs. Reinforcement phases may also experience degradation. For example, mica particles have been reported to undergo exfoliation in mica/Al MMCs.

5.3.1 Aluminum carbide hydrolysis

Aluminum carbide forms by the reaction of aluminum and carbon,[55]

$$4Al(1) + 3C(s) = Al_4C_3(s) \quad [9]$$

and its formation is substantial in Gr/Al MMCs during processing if temperatures are significantly higher than the liquidus temperature. At lower temperatures, Al_4C_3 formation can be controlled.[56]

Aluminum carbide also forms by the reaction of aluminum and SiC,

$$4Al(1) + 3SiC(s) = Al_4C_3(s) + 3Si(s) \quad [10]$$

and has been found at SiC–Al interfaces if the Si activity in liquid aluminum is low.[52]

The formation of Al_4C_3 by the reaction of Al and B_4C is reported to occur rapidly at 900 °C. In addition, many other Al–B–C compounds are known to form.[53]

In the presence of moisture, Al_4C_3 hydrolyzes to liberate methane gas by the reaction

$$Al_4C_3(s)+12H_2O(1) = 4Al(OH)_3(s)+3CH_4(g) \quad [11]$$

Methane evolution has been detected from Al/Gr MMCs containing Al_4C_3.[57,58] The rate of Al_4C_3 hydrolysis was measured to be ~1% per hour for HP Al_4C_3 exposed to pure water at 30 °C.[39] Buonanno[58] reported that Al_4C_3 hydrolysis in Al/Gr MMCs leaves fissures at fiber–matrix interfaces. The hydrolysis of Al_4C_3, therefore, could result in rapid penetration into the MMC microstructures through fiber–matrix interfaces, and lead to the formation of microcrevices at reinforcement–matrix interfaces.

5.3.2 Mica degradation

Muscovite mica $KAl_3Si_3O_{10}(OH)_2$ particles of ~70 μm in size[59] have been used in Al MMCs developed for potential use in applications where good antifriction, seizure resistance, and high-damping capacity are required.[60] During exposure to non-deaerated 3.5 wt% NaCl solutions, the mica particles appeared to have absorbed moisture, swelled, and then exfoliated.[61]

5.4 Secondary Effects

The presence of the reinforcement phases in the MMCs may alter the microstructural features in the matrix material in ways that are nonexistent in the monolithic matrix alloys. Two examples that are discussed here are the formation of intermetallic phases around reinforcements by solute rejection during solidification,[62] and the mismatch in the coefficient of thermal expansion (CTE) between reinforcements and matrices that can lead to dislocation generation,[63] which potentially could lead to higher corrosion in some metals.[64]

5.4.1 Intermetallics

Intermetallics may have potentials and corrosion resistance different from that of the matrix. **Table 3** shows corrosion potentials, pitting potentials, and normal corrosion current densities of various metals and intermetallics.[65] Noble and inert intermetallics may induce galvanic corrosion of the matrix; whereas, active intermetallics may go into dissolution and leave fissures or crevices.

Table 3 Corrosion data[a] of intermetallics

Constituent	E_{corr} *(m V_{SCE})*	E_{pit} *(m V_{SCE})*	i_{corr} *(A cm^{-m})*
Cu (99.9)	−232	−30	1.8×10^{-6}
Si (99.9995)	−441	–	–
Cr (99.0)	−506	297	–
Al_3Fe	−539	106	2.1×10^{-6}
Al_7Cu_2Fe	−551	−448	6.3×10^{-6}
$Al_{20}Cu_2Mn_3$	−565	−428	3.4×10^{-7}
Al–4%Cu	−602	−406	2.3×10^{-6}
Al_3Ti	−603	−225	5.6×10^{-7}
Al_2Cu	−665	−544	7.3×10^{-6}
Al–2% Cu	−672	−471	1.3×10^{-6}
Al_3Zr	−776	−275	2.5×10^{-6}
Al_6Mn	−779	−755	6.3×10^{-6}
$Al_{12}Mn_3Si$	−810	−621	1.7×10^{-6}
Al (99.9999)	−823	−610	3.9×10^{-6}
Al_2CuMg	−883	80	2.0×10^{-6}
Mg (AlCu)	−943	−2	2.3×10^{-5}
7075-T651 Al	−965	−739	1.1×10^{-6}
Zn (99.99)	−1000	–	1.2×10^{-6}
$Al_{32}Zn_{49}$	−1004	–	1.4×10^{-5}
Mg_2Al_3	−1013	−846	4.8×10^{-6}
$MgZn_2$	−1029	–	8.4×10^{-5}
Mn (99.9)	−1323	–	–
Mg_2Si	−1538	–	7.7×10^{-6}
Mg (99.9)	−1586	−1391	5.5×10^{-6}

[a]Aerated, pH 6, 0.1 M NaCl.

Source: Data from Birbilis, N., Buchheit, R.G., 2005. J. Electrochem. Soc. 152 (4), B140–B151.

In Al_2O_3/Al MMCs, Al_8Mg_5 and Mg_2Si, intermetallics provided corrosion paths along fiber–matrix interfaces.[66] Pits in Al_2O_3/Al MMCs exposed to NaCl solutions containing H_2O_2 were attributed to the dissolution of $MgAl_3$, which is rapidly attacked at low potentials.[67] In mica/Al MMCs, a dendritic phase, which was probably Mg_2Al_3 or Al_8Mg_5, and spheroidized $CuMgAl_2$ were preferentially attacked in nondeaerated 3.5 wt% NaCl.[68]

5.4.2 Dislocation density

The high strengths of particulate MMCs in comparison to their monolithic alloys are generated by high dislocation densities caused by a mismatch in the CTE between reinforcement and matrix, and heating and cooling histories.[63] Since cold working, which is the result of generating high dislocation densities, is known to change the corrosion behavior of metals such as steel[64] and aluminum,[69] the corrosion behavior of MMCs may also be affected by high dislocation densities.[33] It has been suggested that corrosion near the SiC–Al interface in SiC/Al MMCs could be caused by high dislocation density because of a mismatch of the CTE between SiC and Al.[70,71]

5.4.3 MMC processing

Processing-induced corrosion is not inherently caused by the primary components of the MMC system, but results from processing deficiencies. The corrosion of diffusion bonds in B/Al MMCs and corrosion due to microstructural chlorides in some Gr/Al MMCs are two examples.

5.4.3.1 Low-integrity diffusion bonds

The open-circuit potentials of Al MMCs reinforced with B MFs were active as that of their monolithic matrix alloys in aerated NaCl solutions,[72,73] which were not expected since B MFs had open-circuit potentials that were noble to that of the monolithic matrix alloy. On the basis of the mixed-potential theory, it was expected that the MMCs would equilibrate at potentials between that of the noble B MF and the monolithic matrix alloy. To investigate the origin of this discrepancy, Bakulin *et al.*[73] measured the open-circuit potentials of HP stacks of aluminum foil processed in the same way as the MMC (but without the B MFs), and found that the HP aluminum stacks were active as that of the monolithic alloy as well as the MMCs. The only difference between the HP stacks of aluminum foil and the monolithic aluminum was crevices in the diffusion bonds between adjacent foils which served as additional anodic sites.

5.4.3.2 Microstructural chlorides

Some types of Gr_F (50%)/Al 6061-T6 MMCs were found to have been contaminated with microstructural chlorides during processing[74] by the Ti–B vapor deposit method[75] that utilizes $TiCl_4$ and BCl_3 gases. The presence of microstructural chlorides in

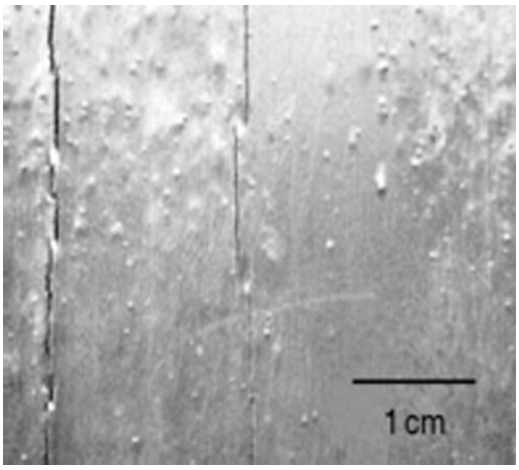

Figure 22 Subcutaneous corrosion in Gr/Al MMC with over 10 years exposure in laboratory air.

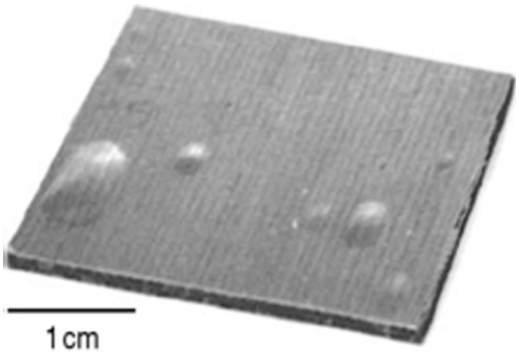

Figure 23 Gr/Mg MMC showing subcutaneous corrosion after more than 15 years in storage.

the Gr/Al MMCs was confirmed during microstructural analyses, and the effect of the chlorides was evident in anodic polarization diagrams.[76] These MMCs are pitted at $\sim -0.6\ V_{SCE}$ in 0.5 M Na_2SO_4[76]; whereas, both the matrix alloy and other types of Gr/Al MMCs are processed by pressure infiltration without the use of chlorides passivate in 0.5 M Na_2SO_4.[58] The residual microstructural chlorides also make these MMCs inherently unstable, and as a result, some specimens have suffered from corrosion initiating subcutaneously beneath monolithic Al skins after long storage in laboratory air (**Figure 22**). This type of subcutaneous corrosion has also been observed in a similar type of Gr/Mg MMC (**Figure 23**).

5.5 Measuring Corrosion of MMCs

5.5.1 Electrochemical techniques

5.5.1.1 Potentiodynamic polarization

The electrochemical methods developed for testing corrosion behavior of monolithic metals and alloys can be also applied to MMCs. The most common technique used is the potentiodynamic polarization that results in polarization curves from which many electrochemical parameters are obtained according to ASTM G 59 and ASTM G 5. However, the corrosion current density (i_{corr}) value, as well as any parameter related to the surface area, has to be dealt with carefulness. The current exerted by MMC constituents is unequal. Therefore, it is difficult to transform the (i_{corr}) values to corrosion rates expressed as weight loss or penetration depth through application of Faraday's law. However, if the reinforcement is insulator as Al_2O_3, the i_{corr} can be correlated to the metal matrix area that equal the total specimen area exposed to corrosion multiplied by the volume fraction of metal matrix.

However, studying the dissolution behavior of MMCs and their individual constituents by anodic polarization measurements leads to valuable results that can reveal a lot of information not only about the electrochemical response of MMCs constituents but also about electrochemical effects evolved by interfacial phases present in the MMCs. The individual anodic polarization diagrams of monolithic metal matrix, reinforcement constituent, and MMC are recorded separately. Then, the individual diagrams of monolithic matrix and of reinforcement are used to generate a hypothetic polarization diagram for the MMC using the

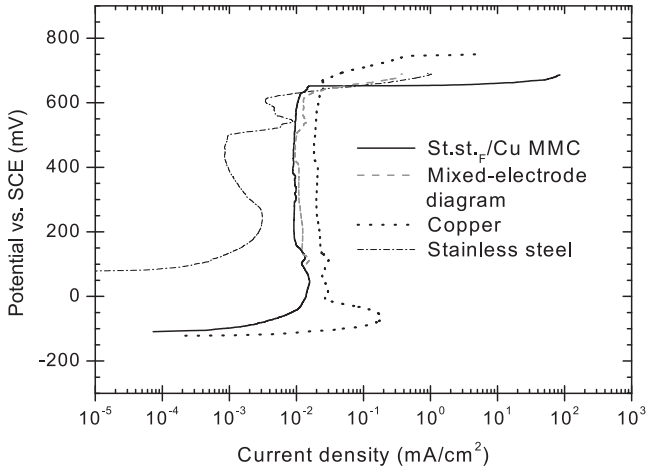

Figure 24 Anodic polarization diagrams of stainless steel $(st.st.)_F$ (50%)/Cu MMC, monolithic copper, and monolithic stainless steel alloy specimens, in addition to a mixed-potential diagram that is generated on the basis of the mixed potential theory for a composite containing 50 vol% stainless steel fibers in copper matrix, in 3% NaCl alkaline solution (pH 11) at 25 °C. Reproduced from Ref. [8]

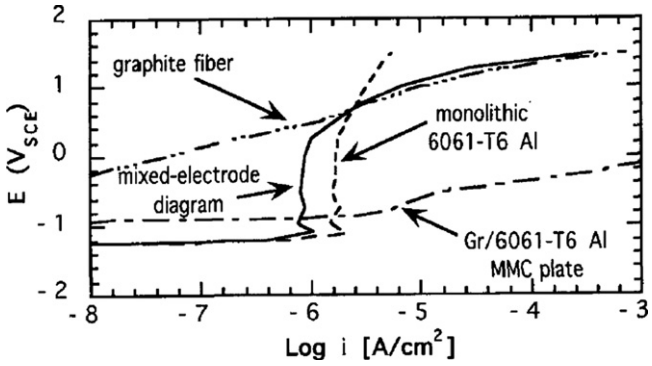

Figure 25 Anodic polarization diagrams of pitch-based graphite fiber, monolithic 6061-T6 aluminum, and Gr(50%)/6061-T6 Al MMC plate in deaerated 0.5 M Na_2SO_4 at 30 °C. The mixed-electrode diagram is generated on the basis of the mixed potential theory for a composite consisting of 50 vol% graphite in 6061-T6 aluminum. Reproduced from Ref. [76].

mixed-potential theory. This latter diagram is called as mixed-electrode diagram. If there is a good consistency between the actual polarization diagram of MMC and the mixed-electrode diagram, the fraction of anodic current exerted by the matrix and that exerted by the reinforcement constituent can be determined. Furthermore, the comparison between the mixed-electrode diagram and the actual polarization diagram of MMC can detect any electrochemical response originating from formation of interphases or contaminants arisen in the MMC microstructure during processing. Following are important examples verifying the assessments resulted from using the anodic polarization technique.

The anodic polarization diagrams of actual stainless $steel_F$ (50%)/copper MMC and the mixed-electrode diagram are in a very high consistence (**Figure 24**). The mixed-electrode diagram is generated from both anodic polarization diagrams of monolithic copper and monolithic stainless steel, in 3% NaCl alkaline solution (pH = 11), on the basis of the mixed-potential theory. The current density calculated for each potential of the mixed-electrode diagram is equal to one half of the current density recorded for copper plus one half of the current density recorded for stainless steel, as the volume fraction (Vf) of stainless steel fibers is 0.5. The very high agreement between the actual polarization diagram and the generated mixed-electrode diagram suggests the possibility to determine the fraction of dissolution current originating from the copper matrix and from the stainless steel fibers. Furthermore, the break-through potential (pitting potential) of the actual MMC is equal to the break-through potential of the mixed-electrode diagram. This indicates the absence of any electrochemical effect of interfacial compound presumably formed at steel/copper interface. Microstructure investigations confirmed the absence of interphases and contaminations may be formed in the MMC due to fabrication and processing.[8]

Contrastingly, a lack of consistency is sometimes found between the anodic polarization diagram of the actual MMC and the mixed-electrode diagram. The dissimilarity in dissolution behavior might be caused by the interphases formed or contaminants introduced in the MMC during fabrication. **Figure 25** shows a mixed-electrode diagram generated from anodic polarization diagrams of graphite fibers and 6061-T6 aluminum alloy in 0.5 M Na_2SO_4 solution.[76] There is a great discrepancy between the

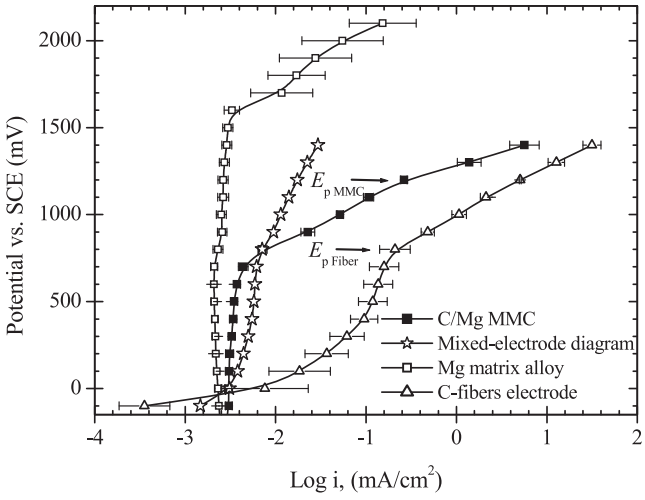

Figure 26 Anodic polarization diagrams of monolithic AS41(0.5Ca) Mg matrix alloy, C-fiber (SG 40) and C_F(25%)/AS41 Mg MMC in 100 ppm NaCl solution (pH=12), in addition to a mixed-potential diagram that is generated on the basis of the mixed potential theory for a composite containing 25 vol% C-fibers in AS41Mg matrix alloy. Reproduced from Ref. [77].

mixed-electrode diagram and the actual polarization diagram of Gr (50%)/6061-T6 Al MMC. The pitting potential of actual MMC is widely shifted to more active potential than that of the mixed-electrode diagram. The pitting potential of MMC is close to its corrosion potential without the passivation behavior depicted by monolithic Al alloy. The accelerated pitting is found to be caused by residual microstructural chloride introduced into the microstructure during processing.[76]

In addition, comparing the anodic polarization behaviors of MMC, matrix alloy, and reinforcement constituent indicates whether the corrosion of MMC is predominantly determined by the metal matrix, or by the reinforcing material. **Figure 26** shows the anodic polarization diagrams of monolithic AS41-Mg matrix alloy, C-fibers and C_F (25%)/AS41-Mg MMC, and a mixed-electrode diagram generated from both anodic polarization diagrams of C-fibers and monolithic Mg-matrix alloy.[77] The comparison of anodic polarization diagrams illustrates many valuable results. Firstly, the gradual increase in the current density of the MMC is due to the increase in the current density for the C-fibers. Secondly, the independence of the pitting potential for the MMC (E_p MMC) on that for the matrix alloy. Thirdly, the discrepancy between the real composite diagram and the generated mixed-electrode diagram after the pitting potential for the C-fiber (E_p Fiber), indicating that the mixed potential theory cannot apply after (E_p Fiber). Consequently, it has been be stated that the polarization behavior of C/Mg MMC is predominantly drawn by the polarization of C-fibers rather than that of matrix alloy, characterizing an invariable pitting potential independent on that of the matrix alloy. Thus, the evidence of pitting C_F/AS41-Mg MMC is induced by the C-fibers. Microstructure investigations[77] showed that the polarization of C-fibers leads to crevice formation along the borders of C-fibers. Consequently, the C/Mg interface is vulnerable to crevice corrosion, which leads to an unexpected pitting potential value within the passive range of monolithic matrix alloy.

5.5.1.2 Galvanic current

Galvanic coupling between the metal matrix and reinforcement is an effective factor in MMC corrosion when the reinforcement material is conductive or semiconductive. For the galvanic current measurements, separate metal matrix and reinforcement electrodes, with equal surface areas, can be coupled through a potentiostat. The galvanic current, flowing through an electrolyte can be measured by using the potentiostat as a zero resistance ammeter (ZRA).[8,77,78] Polarization diagrams can be used to predict the galvanic current; the intersection of the anodic polarization diagram of monolithic metal matrix and the cathodic polarization diagram of reinforcement material represents to the magnitude of galvanic current for a galvanic couple of metal/reinforcement with equal surface area fraction. The difficulty to have a separate electrode from the reinforcement material is a disadvantage of these two techniques aforementioned. Another shortcoming when using these methods is neglect of any microstructural changes caused by MMC processing. However, the two methods can give valuable information about material selection to design a MMC with lower galvanic current arisen between its constituents. The galvanic corrosion current can also be estimated from polarization diagrams of actual MMC and of monolithic metal matrix. The galvanic corrosion current density can be obtained by subtracting the corrosion current density of monolithic metal matrix (namely local corrosion)[78] from the corrosion current density of the actual MMC that has been normalized with respect of matrix area. The three methods illustrated above can be used to estimate the galvanic corrosion behavior. Comparative studies between these methods have been reported.[36,78]

5.5.2 Corrosion in environments

A comprehensive study of Al 6092-T6 MMCs reinforced with black SiC (5, 10, 20, 40, and 50 vol%), green (high purity) SiC (50 vol%), B_4C (20 vol%), and Al_2O_3 (20 vol%) has been examined in a battery of immersion, humidity-chamber exposure, and

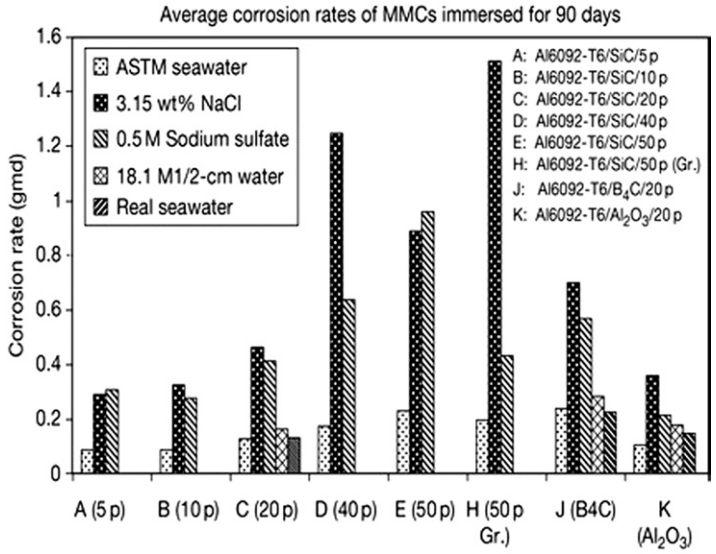

Figure 27 Corrosion rates of Al 6092-T6 MMCs under immersion conditions in air-exposed solutions for 90 days at 30 °C. Reproduced from Hawthorn, G.A., 2004. Outdoor and laboratory corrosion studies of aluminum-metal matrix composites. MS Thesis, University of Hawaii at Manoa, Honolulu.

outdoor exposure tests.[79] The wide range of reinforcement types and testing conditions allows trends in corrosion behavior to be made and will be highlighted here. Since galvanic corrosion between the Al 6092-T6 matrix and reinforcement particles depends on the ability of the particle to conduct electricity, the electronic resistivities of the particle should have an effect on the corrosion behavior. The resistivity of B_4C is $\sim 10^0\ \Omega$ cm,[45] that of SiC ranges from $\sim 10^{-5}$ to $10^{13}\ \Omega$ cm depending on its purity,[40] and that of Al_2O_3 is $10^{14}\ \Omega$ cm.[42] The green SiC possessing high electrical resistivity should be less likely to promote galvanic corrosion of the aluminum matrix as compared to black SiC, which is of lower purity and resistivity.

5.5.2.1 *Immersion exposure*

Immersion studies were conducted for 90 days in 3.15 wt% NaCl, ASTM seawater, real seawater, 0.5 M Na_2SO_4, and ultrapure 18 Ω cm water exposed to air at 30 °C. The dimensions of the specimens were $\sim 2.54\ \text{cm} \times 2.54\ \text{cm} \times 0.25\ \text{cm}$. Specimens in triplicate were examined, but data correspond to results from two specimens for each testing condition (**Figure 27**). The third specimen was reserved for further surface analyses.

Corrosion rates were generally highest for the MMCs immersed in 3.15 wt% NaCl. The rates were much lower in ASTM seawater because of the formation of a film on the MMC surfaces, which was likely composed of Al–Mg hydrotalcite-like compounds.[80] The film may have impeded the diffusion of dissloved oxygen to cathodic regions limiting the corrosion rate. For most of the specimens, the corrosion rates in Na_2SO_4 were similar to those in NaCl. Although Al MMCs generally passivate in Na_2SO_4 solutions during anodic polarization, they corrode in the open-circuit condition because of the formation of localized acidic and alkaline regions (see Section 5.1.7).

Most of the trends observed in the corrosion rate versus the reinforcement composition and type indicated that the level of galvanic corrosion between the matrix and reinforcements increases as the reinforcement electrical resistivity decreases, and as the reinforcement content increases. For the MMCs with 20 vol% of particulates, the corrosion rates were generally highest for that reinforced with B_4C, followed by that with black SiC, and least for that with Al_2O_3. Of the three types of reinforcements, the B_4C has the lowest electrical resistivity, and Al_2O_3 has the highest. For the MMCs reinforced with 5, 10, 20, 40, and 50 vol% black SiC, the corrosion rates also generally increased as the volume fraction increased. For the MMCs reinforced with 50% black or green SiC, corrosion rates were higher for those that were reinforced with the lower purity, more conductive, black SiC in ASTM seawater and 0.5 M Na_2SO_4. It was expected that this trend would also be observed for the 3.15 wt% NaCl solution, but the results in this solution were skewed because of crevice and localized corrosion on one of the MMCs reinforced with the higher-purity, less-conductive, green SiC. A crevice formed on the specimen because of contact with the specimen holder, and a highly localized corrosion site formed in a region of high plastic deformation where the specimen was stamped for identification.

5.5.2.2 *Humidity chamber exposure*

Humidity chamber studies were conducted for 90 days at 85% RH (relative humidity) and 30 °C. The dimensions of specimens were $\sim 2.54\ \text{cm} \times 2.54\ \text{cm} \times 0.25\ \text{cm}$. The specimens were treated in 3.15 wt% NaCl, ASTM seawater, actual seawater, and 0.5 M Na_2SO_4 by immersion in the electrolyte for 1 min, air-dried, and then placed in the humidity chamber. Specimens in triplicate

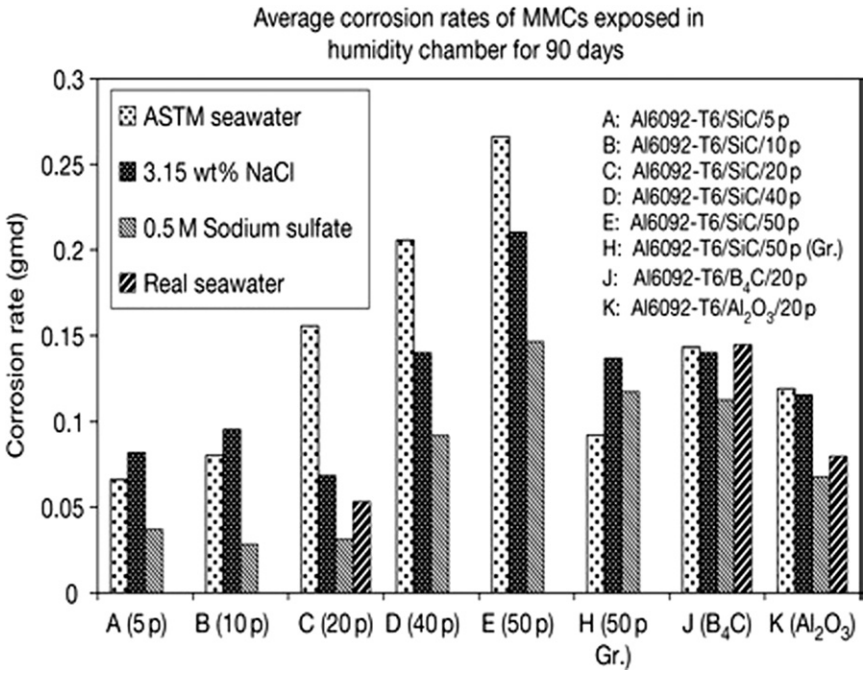

Figure 28 Corrosion rates of Al 6092-T6 MMCs treated with various salts and exposed to 85% RH for 90 days at 30 °C. Reproduced from Hawthorn, G.A., 2004. Outdoor and laboratory corrosion studies of aluminum-metal matrix composites. MS Thesis, University of Hawaii at Manoa, Honolulu.

were examined, but data correspond to results from two specimens for each testing condition (Figure 28). The third specimen was reserved for further surface analyses.

The corrosion rates of specimens treated with ASTM seawater were generally comparable to or exceed those treated with NaCl, as the hydrotalcite-like films cannot form in the absence of an electrolyte. The specimens treated with Na_2SO_4 generally had the lowest corrosion rates. Corrosion rates also generally increased for the MMCs reinforced with black SiC as the SiC content increased. For the MMCs reinforced with 50 vol% SiC, corrosion rates were lower for those having the high-purity, higher resistivity, and green SiC.

5.5.2.3 Outdoor exposure

The MMC specimens were exposed to six outdoor sites. The specimens were ~9 cm in diameter and 2.5 mm in thickness. Specimens in triplicate were examined, but data correspond to results from two specimens for each testing condition (Figure 29). The third specimen was reserved for further surface analyses.

The test sites were industrial (Campbell Industrial Park), agricultural (Ewa Nui), arid (Waipahu), marine (Kahuku and Coconut Island sites), and rain forest (Lyon Arboretum). Weather and environmental data are provided for the 180-day exposure period (Table 4).

Some trends are clearly visible in the corrosion data (Figure 29). The corrosion rates of the MMCs reinforced with black SiC generally increased with an increase in volume fraction of the reinforcement. This would be expected due to galvanic action between the black SiC and aluminum matrix. For the MMC reinforced with 50 vol% SiC, those having the black SiC corroded at higher rates than those reinforced with the high-purity, higher-resistivity, and green SiC. For the three types of MMCs with 20 vol% particulates, those reinforced with B_4C generally corroded at a higher rate than those reinforced with less-conductive SiC or Al_2O_3.

The highest corrosion rates were generally observed at the Manoa (very wet), Coconut Island (marine), and Kahuku (marine) test sites. The high corrosion rate at Manoa is likely due to persistent rain since chloride levels are negligible at that site.

5.5.2.4 Hydrogen evolution test

The free immersion test can be applied for short or long times to measure the corrosion rate of MMCs in environments of interest. The weight loss should be determined after cleaning the corroded surfaces from corrosion products. The fiber-reinforced MMCs may develop deep pits which entrap corrosion products and corrosion solution. This may cause a difficulty to get accurate weight of corroded MMC specimens. Therefore, hydrogen evolution test was preferred for comparison of corrosion rates of some Mg MMCs and their matrix alloys,[77,81] where hydrogen reduction is the cathodic reaction in Mg corrosion. However, microscopic observations of initially corroded MMC surfaces after immersion for short times show whether the precursors of corrosion sites arise at, close to, or away from reinforcement/metal interface.[8,77,81] In addition, cross-sectional observation of corroded MMC specimens demonstrate the propagation behavior of corrosion sites.

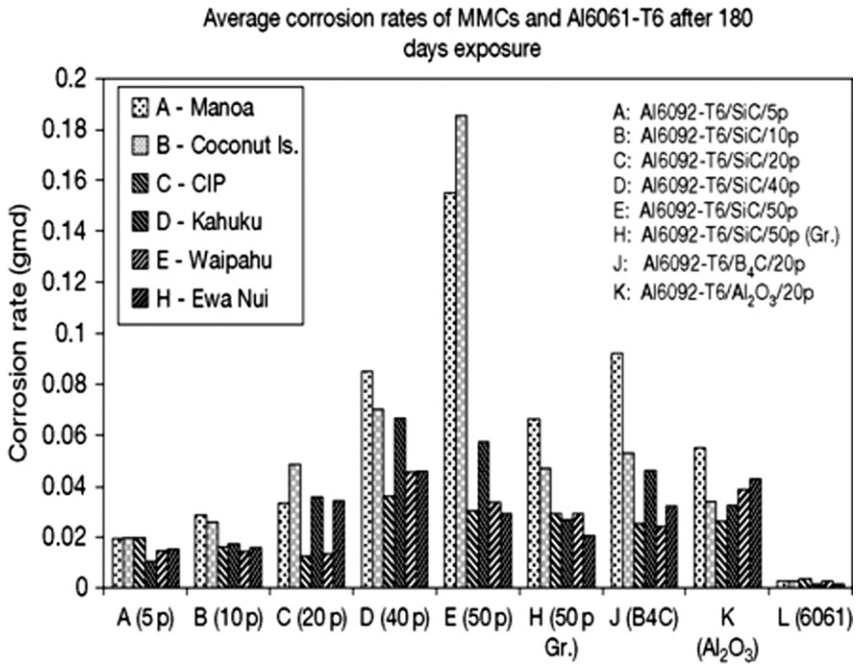

Figure 29 Corrosion rates of Al 6092-T6 MMCs exposed to outdoor test sites for 180 days. Reproduced from Hawthorn, G.A., 2004. Outdoor and laboratory corrosion studies of aluminum-metal matrix composites. MS Thesis, University of Hawaii at Manoa, Honolulu.

Table 4 Weather and atmospheric data for 180-day exposure at test sites

Test site	*Avg. temp (°C)*	*Rain (cm)*	*% of exposure time when TOW = 0*[a]	*% of exposure time when TOW = 15*[a]	*Avg. Cl^- deposition rate (mg m^{-d} day^{-a})*	*Avg. humidity (%RH)*
Manoa	22.9	357.9	60.6	26.4	–[b]	83.1
Coconut Is.	25.8	65.0	54.8	9.2	58.3	74.9
Campbell	27.2	45.5	66.5	4.6	24.4	63.2
Kahuku	25.6	132.1	59.6	15.1	89.9	73.4
Waipahu	26.3	79.0	80.3	7.1	10.7	66.9
Ewa Nui	25.9	82.6	77.6	6.5	9.4	67.4

[a]A TOW sensor value of zero indicates that the specimens are dry and a value of 15 indicates that the specimens are wet.
[b]Below detectable level of 7.0.
Source: Hawthorn, G.A., 2004. Outdoor and laboratory corrosion studies of aluminum-metal matrix composites. MS Thesis, University of Hawaii at Manoa, Honolulu.

5.5.3 Mechanically assisted corrosion

Few studies on stress corrosion cracking (SCC) behavior, as well as on corrosion fatigue, of MMCs have been reported.[82] The testing programs that have been developed for SCC and corrosion fatigue of pure metals and alloys can be used for testing MMCs with emphasis on the role of reinforcement constituent. Fractography and scanning electron microscopy studies on SiO_2–Al_2O_3 fiber-reinforced aluminum MMCs were important to reveal that SCC is controlled by dissolution and hydrogen embrittlement mechanisms.[83] The study showed that pitting occurs preferentially at the fiber/matrix interfaces.[83] $Al_2O_{3\ CF}$/ZE41 Mg MMC specimens stressed parallel to the fiber axis in NaCl–K_2CrO_4 solution retained approximately 90% of the strength in air. However, the MMC with the stress aligned perpendicular to the fiber axis retained only 40–60% of the strength in air.[84] If the reinforcement constituent is non-conductive, like Al_2O_3, and does not form any interfacial compound with the matrix alloy, then there should not be any galvanic effect on the corrosion of MMC. Thus, the reinforcement may have not any deleterious impact on the general corrosion resistance of MMC. Nevertheless, the reinforcement can adversely influence the SCC behavior of such composite system through piling up of dislocations near hard reinforcement/matrix interfaces.[85] Other ways by which the discontinuous reinforcement can significantly affect on the SCC of Al MMCs have been studied and reviewed.[85]

Corrosion fatigue behavior of MMCs is affected by type of reinforcement and processing conditions. The corrosion–fatigue cracking rate is influenced by loading frequency, stress amplitude, and the loading direction relative to reinforcement direction and relative to extrusion or rolling direction.[86] The fatigue fracture behavior under combined tension–torsion loading of a SiC whiskers (SiC_w)-reinforced aluminum alloy MMCs was investigated in 3.5% NaCl solution.[87] The nucleation of crack was found to initiate

at corrosion pits formed on the surface of composite specimen.[87] The reinforcement shape has a significant effect on corrosion fatigue, as well as on SCC. The crack propagation rates are reduced by increasing the length-to-diameter ratio of reinforcement.[88] This is in agreement with the finding that Al MMC reinforced with SiC whiskers has longer corrosion fatigue live than that reinforced with SiC paricles.[89] A brief review of studies on SCC and corrosion fatigue of Al MMCs has been recently reported.[90]

5.6 Corrosion Protection of MMCs

Corrosion of metals can be controlled or prevented by surface modification or by application of appropriate protective coating. Surface modification techniques involve the change of chemical composition and thus the chemical and physical properties of the metal outer surface. The most known examples for these techniques are anodization and conversion coating. Protective coating is mostly effective to prevent corrosion of metal substrates through providing a barrier between the metal and its environment. Examples of possible coating technologies available for metallic substrates are electroplating, thermal spray coating, laser cladding, chemical vapor deposition (CVD), physical vapor deposition (PVD), and polymer coating. For MMCs, however, a proven coating system for the matrix alloy may not be suitable. Poor adhesion and wettability between the coating and reinforcement or differences in the electrochemical properties of the alloy and the MMC may render a good coating system for the alloy ineffective for the MMC. Other coating techniques such as anodization could also be ineffective or even deleterious to the MMC. Thermal spray coating and laser cladding can be applied effectively, but a particular concern has to be paid to the difference of thermal properties between the MMC constituents and the coat/metal and coat/reinforcement interfaces have to be studied.[91,92] Various studies on the corrosion protection of MMCs utilizing organic coatings, inorganic coatings, anodization, chemical conversion coatings, and inhibitors have been summarized elsewhere.[93]

6 Conclusions

The corrosion of MMCs is significantly more complicated and less predictable than that of their monolithic alloys. MMC systems that consist of active metal matrices and noble reinforcements have inherent galvanic corrosion problems. Some systems, such as those containing aluminum and carbon, may also be susceptible to interphase formation of the deleterious Al_4C_3, which hydrolyzes in the presence of moisture. Other complications arise when reinforcements are semiconductors, which have electrical resitivities that can span orders of magnitude and are sensitive to impurity levels. In addition, impurities in semiconducting reinforcements may cause them to become n-type or p-type which can lead to photo-induced corrosion or even beneficial photoinduced cathodic protection. The presence of the reinforcements may also influence the formation of intermetallics and the generation of dislocations, which also affect corrosion behavior. These additional concerns make designing and utilizing MMCs a significant, but worthy, engineering challenge. Many of the extraordinary mechanical and physical properties of MMCs cannot be achieved with conventional metal alloys. Standardization of MMC constituents (e.g., purity levels in reinforcements) and the stringent control of processing temperatures and histories could help develop MMCs with more predictable corrosion behavior.

References

1. Weeton, J.W., Peters, D.M., Thomas, K.L., 1987. Guide to Composite Materials. Metals Park, OH: American Society for Metals.
2. Park, G.B., Foster, D.A., 1990. International Technical Conference Proceedings, SUR/FIN'90, Boston, MA, July 1990, pp. 1349–1369. Boston, MA, American Electroplaters and Surface Finishers Society.
3. Harrigan, W.C.J., 1991. Metal Matrix Composites, Processing and Interfaces. Academic Press, pp. 1–16.
4. Liu, Y., Rohatgi, P.K., Ray, S., *et al.*, 1991. Conference Proceedings, ICCM/8. Society for the Advancement of Material and Process Engineering (SAMPE) 20H.
5. Lim T., Lee C.S., Kim Y.H., *et al.*, 1991. Conference Proceedings, ICCM/8. Society for the Advancement of Material and Process Engineering (SAMPE) 20E.
6. Ashby, M.F., Jones, D.R.H., 1998. Engineering Materials, vol. 2, second ed., Butterworth Heinemann.
7. Vassel, A., 1999. Mater. Sci. Eng. A 263, 305–313.
8. Bakkar, A., Ataya, S., 2014. Corros. Sci. 85, 343–351.
9. Walker, J.C., Rainforth, W.M., Jones, H., 2005. Wear 259, 577–589.
10. Guo, M.-H., Liu, J.Y., Li, Y.-X., 2014. Trans. Nonferrous Met. Soc. China 24, 1039–1045.
11. Mondal, A.K., Kumar, S., 2009. Composites Sci. Tech. 69, 1592–1598.
12. Bahgat, R.B., 1991. Metal Matrix Composites: Processing and Interfaces. Academic Press, pp. 43–82.
13. Chawla, K.K., 1993. Structure and Properties of Composites. Vch Verlagsgesellshaft GmbH Co., pp. 121–182.
14. Willis, T.C., 1988. Metals Mater. 4, 485–488.
15. Everett, R.K., 1991. Metal Matrix Composites: Processing and Interfaces. Academic Press, pp. 103–113.
16. Rack, H.J., 1991. Metal Matrix Composites: Processing and Interfaces. Academic Press, pp. 83–101.
17. Everett, R.K., 1991. Metal Matrix Composites: Processing and Interfaces. Academic Press, pp. 17–42.
18. Buck, M.E., Suplinskas, R.J., 1987. Engineered Materials Handbook on Composites, vol. 1. Metals Park, OH: ASM International, pp. 851–857.
19. Surappa, M.K., 2003. Sadhana 28 (1–2), 319–334.
20. Adebisi, A.A., Maleque, M.A., Rahman, M.M., 2011. Int. J. Automotive Mech. Eng. 4, 471–480.
21. Chawla, N., Chawla, K.K., 2013. Metal Matrix Composites. Springer, pp. 325–355.

22. Lecouturier, F., Spencer, K., Thilly, L., Embury, J.D., 2004. Physica B 346–347, 582–588.
23. Macke, A., Schultz, B.F., Rohatgi, P., 2012. Adv. Mater. Processes 170 (30), 19–23.
24. DWA Technologies Inc., 2015. Available at: http://dwatechnologies.com (accessed 26.11.15).
25. Rajabi, A., Ghazali, M.J., Syarif, J., Daud, A.R., 2014. Chem. Eng. J. 255, 445–452.
26. Wesley, W.A., Brown., R.H., Uhlig, H.H., 1948. The Corrosion Handbook, first ed. New York: Wiley. pp. 481–495.
27. Hihara, L.H., Kondepudi, P.K., 1994. Corros. Sci. 36, 1585–1595.
28. Hihara, L.H., Latanision, R.M., 1992. Corrosion 48 (7), 546–552.
29. Lin Z.J., 1995. Corrosion study of silicon-aluminum metal-matrix composites. MS Thesis, University of Hawaii at Manoa, Honolulu.
30. Tamirisa C., 1993. Corrosion behavior of silicon-carbide reinforced titanium 15-3 metal-matrix composite in 3.15 wt% NaCl. MS Thesis, University of Hawaii at Manoa, Honolulu.
31. Hihara, L.H., Tamirisa, C., 1995. Mater. Sci. Eng. A 198, 119–125.
32. Hihara, L.H., Latanision, R.M., 1994. Int. Mater. Rev. 39, 245–264.
33. Hihara, L.H., 1997. Corros. Rev. 15 (3–4), 361–386.
34. Ding, H., Hihara, L.H., 2008. ECS Trans. 11 (18), 41–52.
35. Ding, H., Hihara, L.H., 2008. ECS Trans. 11 (15), 109–120.
36. Ding, H., Hihara, L.H., 2010. J. Electrochem. Soc. 157 (2), C79–C85.
37. Adler, R.P.I., Snoha, D.J., Hawthorn, G., Hihara, L.H., Beatty, J., 2005. Characterization of environmentally exposed aluminum metal matrix composite corrosion products as a function of volume fraction and reinforcement specie. Paper 06T029 Tri Serice Corrosion Conference, Orlando, FL.
38. Ding, H., Hihara, L.H., 2008. J. Electrochem. Soc. 155 (5), C226–C233.
39. Hihara L.H., 1989. Corrosion of metal matrix composites. PhD Thesis, Massachusetts Institute of Technology, Cambridge, MA.
40. Ichinose, N., 1987. Introduction to Fine Ceramics. John Wiley and Sons, pp. 50–52.
41. Tsirlin, A.M., Watt, W., Perov, B.V., 1985. Strong Fibres (Handbook of Composites), vol. 1. Elsevier Science Publishers, pp. 155–199.
42. Bolz, R.E., Tuve, G.L., 1973. CRC Handbook of Tables for Applied Engineering Science, second ed. Boca Raton, FL: CRC Press, pp. 262–264.
43. Clauser, H.R., 1963. The Encyclopedia of Engineering Materials and Processes. Reinhold Publishing Corporation, p. 429.
44. Greenwood, N.N., Earnshaw, A., 1984. Chemistry of the Elements. Pergamon Press.
45. Yamada, S., Hirao, K., Yamauchi, Y., Kanzaki, S., 2003. Ceram. Int. 29, 299–304.
46. Weeton, J.W., Peters, D.M., Thomas, K.L., 1987. Guide to Composite Materials. Metals Park, OH: American Society for Metals, pp. 5–10.
47. Evans, R., 1937. Metallic Corrosion, Passivity and Protection. London: Edward Arnold and Co., pp. 513–516.
48. Hihara L.H., Devarajan T.S., Ding H., Hawthorn G.A., 2005. Corrosion Initiation and Propagation in Particulate Aluminum-Matrix Composites Tri-Service Corrosion Conference, Orlando, FL, 14–18 November 2005.
49. Hihara L.H., Lin Z.J., 1999. Seventh Japan International SAMPE Symposium and Exhibition, Tokyo, Japan.
50. Deltombe, E., Vanleugenhaghe, C., Pourbaix, M., 1974. Atlas of Electrochemical Equilibria in Aqueous Solutions. Houston, TX: National Association of Corrosion Engineers. pp. 168–176.
51. Ding, H., Hihara, L.H., 2005. J. Electrochem. Soc. 152 (4), B161–B167.
52. Iseki, T., Kameda, T., Maruyama, T., 1984. J. Mater. Sci. 19, 1692–1698.
53. Grytsiv, A., Rogl, P., 2004. Light Metal Systems. Part 1: Selected Systems from Ag–Al–Cu to Al–Cu–Er, 11A1. Berlin, Heidelberg: Springer.
54. Pohlman, S.L., 1978. Corrosion 34, 156–159.
55. Becher, H.J., Brauer, G., 1963. Handbook of Preparative Inorganic Chemistry, vol. 1, second ed., Academic Press, p. 832.
56. Kendall., E.G., Kreider, K.G., 1963. Metal Matrix Composites. New York: Academic Press. vol. 4, pp. 319–397.
57. Portnoi, K.I., Timofeeva, N.I., Zambolotskii, A.A., *et al*., 1981. Poroshkovaya Metallurgiya 218 (2), 45–49.
58. Buonanno, M.A., 1992. PhD Thesis, Massachusetts Institute of Technology, Cambridge, MA.
59. Deonath, S.K., Bhat, R.T., Rohatgi., P.K., 1980. J. Mater. Sci. 15, 1241–1251.
60. Rohatgi, P.K., Asthana, R., Das, S., 1986. Int. Mater. Rev. 31, 115.
61. Deonath, S.K., Namboodhiri, T.K., 1988. Composites 19, 237–243.
62. Mortensen, A., Cornie, J.A., Flemings, J., 1988. J. Met. 40 (2), 12–19.
63. Arsenault., R.J., Everett, R.K., Arsenault, R.J., 1991. Metal Matrix Composites: Mechanisms and Properties. New York: Academic Press, p. 79.
64. Uhlig, H.H., Revie, R.W., 1985. Corrosion and Corrosion Control, third ed. New York: Wiley, p. 123.
65. Birbilis, N., Buchheit, R.G., 2005. J. Electrochem. Soc. 152 (4), B140–B151.
66. Bruun N.K., Nielsen K., Hansen J.Y., 1991. Metal Matrix Composites-Processing, Microstructure and Properties. 12th Riso International Symposium on Materials and Science, pp. 257–264.
67. Yang J.-Y., Metzger M., 1991. Extended Abstracts, vol. 81–82, The Denver, CO: Electrochemical Society. Abstract no. 115.
68. Deonath, S.K., Namboodhiri, T.K., 1989. Corros. Sci. 29, 1215–1229.
69. Butler, G., Ison, H.C.K., Robert, E., 1978. Corrosion and its Prevention in Waters. New York: Krieger Publishing, p. 149.
70. Ahmad, Z., Paulette, P.T., Aleem, B.J.A., 2000. J. Mater. Sci. 35, 2573–2579.
71. Yao, H.-Y., Zhu, R.-Z., 1998. Corrosion 54 (7), 499–503.
72. Sedriks, A.J., Green, J.A., Novak, D.L., 1971. Metall. Trans. 2, 871–875.
73. Bakulin, A.V., Ivanov, V.V., Kuchkin, V.V., 1978. Zaschita Metallov. 14 (1), 102–104.
74. Hihara, L.H., Latanision, R.M., 1990. Mater. Sci. Eng. A 126, 231–234.
75. Harrigan, W.C.J., Flowers, R.H., Cornie, J.A., Crossman, F.W., 1979. Failure Modes in Composites, vol. IV. Warrendale, PA: The Metallurgical Society of AIME, pp. 319–335.
76. Hihara, L.H., Latanision, R.M., 1991. Corrosion 47, 335–341.
77. Bakkar, A., Neubert, V., 2009. Electrochim. Acta 54, 1597–1606.
78. Hihara, L.H., Kondepudi, P.K., 1993. Corros. Sci. 34, 1761–1767.
79. Hawthorn G.A., 2004. Outdoor and laboratory corrosion studies of aluminum-metal matrix composites. MS Thesis, University of Hawaii at Manoa, Honolulu.
80. Ding, H., Hawthorn, G.A., Hihara, L.H., 2008. ECS Trans. 6 (24), 29–40.
81. Bakkar, A., Neubert, V., 2007. Corros. Sci. 49, 1110–1130.
82. Hihara, L.H., 2005. Metal-matrix composites. In: Baboian, R. (Ed.), Corrosion Tests and Standards: Application and Interpretation, second ed. West Conshohocken, PA: ASTM International, pp. 637–655.
83. Winkler, S.L., Flower, H.M., 2004. Corros. Sci. 46, 903–915.
84. Evans, J.T., 1986. Acta Metall. 34, 2075–2083.
85. Singh, P.M., Lewandowski, J.J., 1996. J. Mater. Sci. Letters 15, 490–493.
86. Buck, R.F., Thompson, A.W., 1991. Environmental fatigue in Al-SiC composites. In: Jones, R.H., Ricker, R.E. (Eds.), Environmental Effects on Advanced Materials. Warrendale, PA: The Minerals, Metals, and Materials Society, pp. 297–313.

87. Minoshima, K., Nagashima, I., Komai, K., 1998. Fatigue and Fracture of Engineering Materials and Structures 21, 1435–1446.
88. Jones, R.H., 1991. Stress corrosion cracking of metal matrix composites: Modeling and experiments. In: Jones, R.H., Ricker, R.E. (Eds.), Environmental Effects on Advanced Materials. Warrendale, PA: The Minerals, Metals, and Materials Society, pp. 283–295.
89. Hasson, D.F., Crowe, C.R., Ahearn, J.S., Cooke, D.C., 1984. Fatigue and corrosion fatigue of discontinuous SiC/Al metal matrix composites. In: Early, J.G., Shives, T.R., Smith, J.H. (Eds.), Failure Mechanisms in High Performance Materials. New York: Cambridge University Press, pp. 147–156.
90. Hihara, L.H., 2014. Metal matrix composites. In: Hihara, L.H., Adler, R.P.I., Latanision, R.M. (Eds.), Environmental Degradation of Advanced and Traditional Engineering Materials. Boca Raton, FL: CRC Press, pp. 297–336.
91. Bakkar, A., Galun, R., Neubert, V., 2005. Lasers Eng. 15 (1–2), 63–73.
92. Bakkar, A., Galun, R., Neubert, V., 2006. Mater. Sci. Technol. 22, 353–362.
93. Hihara, L.H., Cramer, S.D., Covino, J., 2005. ASM Handbook, Corrosion: Materials, vol. 13B. Materials Park, OH: ASM International, pp. 538–539.